Doctor of Philosophy

Multiple functional polymer composites employed as binders for Lithium-ion battery electrodes

The Graduate School of the University of Ulsan

Department of Chemical Engineering

Mi Tian

Multiple functional polymer composites employed as binders for Lithium-ion battery electrodes

Supervisor Professor Eun-Suok Oh

A Dissertation

Submitted to

The Graduate School of the University of Ulsan

In partial Fulfillment of Requirements for the Degree of Doctor of Philosophy

By

Mi Tian

Department of Chemical Engineering and Bioengineering

July 2024

Multiple functional polymer composites employed as binders for Lithium-ion battery electrodes

Thesis for the degree of Doctor of Philosophy

by

Mi Tian

has been approved

Committee Chair Prof. Sung Gu Kang

Committee Member Prof. Won Mook Choi

Committee Member Prof. Jun-Bom Kim

Committee Member Prof. Wenjun Gan

Committee Member Prof. Eun-Suok Oh

Department of Chemical Engineering and Bioengineering

University of Ulsan

Abstract

Lithium-ion batteries (LIBs) have extended their application from small portable devices to electric vehicles (EV) and energy storage systems (ESS). The urgent demand for electric vehicles and the rapid consumption of LIBs requires it with high energy densities, environmental friendliness, and resource sustainability. Typically, Silicon (Si) materials are considered as an ideal anode active material for next-generation LIB, due to its advantages of high theoretical capacity (~4200 mAh/g), low operation potential (< 0.5 V vs. Li/Li^+), and abundant resources. Cathode active materials, nowadays, are expected with wide working potential to increase LIB's energy density. Such as high-voltage spinel cathode materials, layered oxide cathode Materials etc. However, there are several imperative issues for the LIBs: high energy density, prolonged cycle stability, excellent rate capability, low cost, safety, and environmental-friendly manufacturing process. To cope with the issues, many researchers have made effective efforts on it. All components of LIBs electrodes have been studied to optimize their performance according to their application. Although binders normally used in a small amount, play a crucial role in maintaining electrode structure integral. The commercially used binder divided into two types, organic-based polyvinylidene fluoride (PVDF), and water-based styrene-butadiene rubber (SBR). However, the traditional PVDF binder, which interacts with electrode materials via weak Van der Waals forces and consequently

lacks the necessary capabilities, could not fulfill the high demands of batteries with high energy density. Besides, PVDF needs to dissolve into NMP organic solvent during slurry preparation process. that causes environment problems. SBR is more environmental friendliness but could not use under high voltage situations and lacks more functions like ionic conductivity, electrical conductivity, mechanical properties and so on.

In view of the above-mentioned shortcomings in the research of binders for LIBs, in this article. A variety of new binders for LIBs were designed and synthesized to improve LIB's performance. The main research contents and results are summarized as follows:

(1) A new polyacrylate latex (PAL) as binder was applied for high voltage cathode in LIBs. One of the biggest advantages of the polyacrylate binder is that it is electrochemically stable at the working voltage of typical cathodes (> 4.5 V vs. Li/Li^+), unlike a conventional water dispersed SBR. Though PVDF is electrochemically stable under high voltage, but it could not alleviate fast capacity decay and unable to be stable under high current density. In contrast, the $LiFePO_4$ (LFP) cathode containing the PAL binder could achieve an excellent specific discharge capacity of 155 mAh g^{-1} with a high-capacity retention of 91.5% after 100 cycles at 1.0 C. Even the specific discharge capacity remains at more than 50% when the charge/discharge current density increases up to 10 C.

(2) MXene clay (Ti2C)-containing in-situ polymerized hollow core-shell composite binder was used as binder for enhancing electrical conduction of silicon anode. In this work a new water-based binder, MXene clay/hollow core-shell acrylate composite (MC-HCS), was synthesized through an in-situ emulsion polymerization technique to alleviate the fast capacity fading of the silicon anode efficiently. The introduction of conductive MXene clay and the hollow core-shell structure, favorable to electrons and ions transport in silicon-based electrodes, gives a novel conceptual design of the binder material. Such a strategy could alleviate electrical isolation after cycling and promise the better electrochemical performance of the high-capacity anodes. The MXene clay/hollow core-shell acrylate binder exhibits high-capacity retention of 1351 mAh g-1 at 0.5 C after 100 cycles and good rate capability over 1100 mAh g^{-1} at 5 C.

(3) Tannic acid (TA) cross-linked poly (vinyl alcohol) (PVA) and poly (sulfobetaine methacrylate-co-Acrylamide) (SBAAm) abbreviated as TA-c-PVA/SBAAm was used as water-dispersed binder for silicon/graphite (Si/C) anodes in LIB. In this work, sulfobetaine methacrylate (SBMA) is a kind of zwitterionic monomers, which can provide single direction ionic conductivity. PVA and PAAm could provide good mechanical properties. TA in this work was used as cross linker to construct a 3D network. Chemical crosslinking could improve the mechanical strength of the binder, which ensure silicon-based electrodes integral during huge

volume change. The Si/C electrodes constructed by TA-c-PVA/SBAAm binder demonstrates a stable long-term cycle performance at 0.5C and high-capacity retention of around 800 mAh g^{-1}.

Table of Contents

List of tables

List of figures

1 Chapter 1 introduction

1.1 Lithium-ion batteries (LIBs)

Battery is a system that could transfer chemical energy into electrical energy through electrochemical reactions. Two types of batteries were developed over past years and could be classified as primary (non-rechargeable) or secondary (rechargeable) batteries. The primary battery generates current by chemical reaction, the active materials also consumed during operation, thus the reaction during primary batteries operation is irreversible and the energy could not be continuously generated. In contrast, the secondary batteries could charge and discharge by switching the current direction, the active materials could be recyclable through restoring and releasing ions. LIBs are one of rechargeable batteries. Compared with many other types of batteries, LIBs with variety of advantages such as high energy density, low self-discharge rate, higher voltage level, light weight etc. currently occupy dominant position in consumer electronics, power tools etc.

1.1.1 The development of LIBs

Figure 1-1 briefly describes the history of LIBs development. Looking back to 1970s, the first rechargeable battery was demonstrated by Whittingham[1]. It was driven by lithium ions and consisted of lithium metal as anode and a titanium disulphide (TiS_2) as cathode. Following that, a layered structure $LiCoO_2$ cathode was discovered by Goodenough's group in 1980, which increased the working voltage

level from 2.5 V to 4 V[2]. Furthermore, in 1985, the prototype of current lithium-ion batteries was designed by Akira Yoshino[3]. They replaced the lithium-melt with petroleum coke as anode. and then a Japan's corporation, Sony, first achieve the commercialization of LIBs by pairing graphite as anode and $LiCoO_2$ as cathode. as the 2019 noble prize in chemistry awarded to John B. Goodenough, M. Stanley Whittingham and Akira Yoshino for their contributions in the development of LIBs, it becomes more and more popular and occupies a dominant position in batteries market. Nowadays, LIBs still are dominant in the market of batteries from portable devices to electric vehicles.

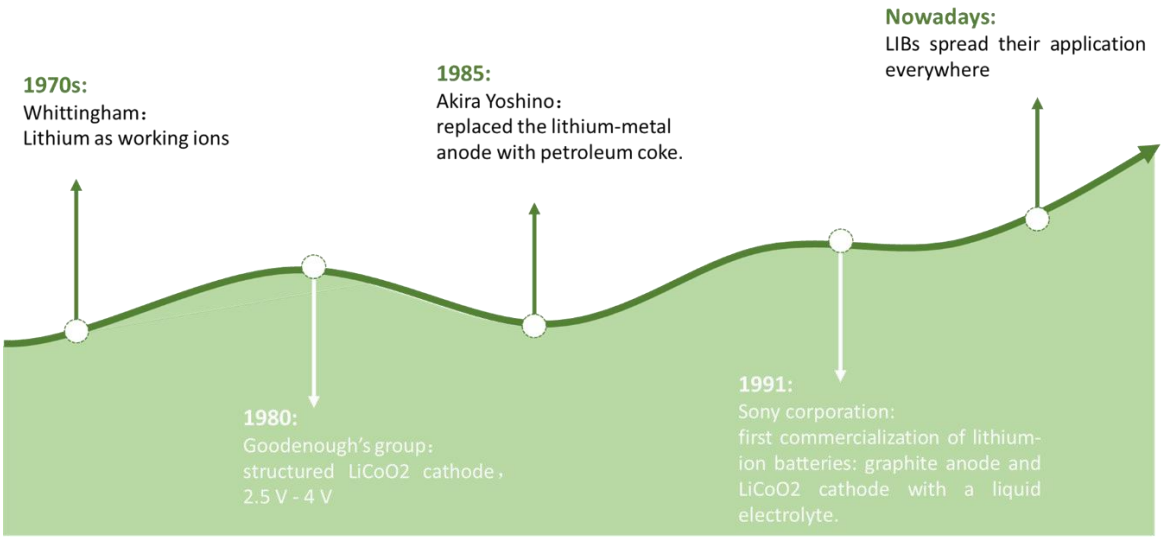

Figure 1-1 The brief history of LIBs development

1.1.2 Working principle

As figure 1-2 shows, LIBs are composed of cathode, anode, electrolyte and separator. In the beginning, the lithium ions store in cathode materials, so cathode also be called the sources of lithium ions. The anode receives and stores lithium ions from cathode. Between two electrodes, electrolyte liquids help the lithium ions shuttle during battery operation. The separator blocks the flow of negative and positive electrons inside the battery and allows ions to pass through, what's more, it avoids two electrodes contact and causes short circuit.

The operational principle of secondary Li-ion batteries is based on reversible redox reaction. During charging, it transfers the electrical energy into chemical energy and store lithium ions from cathode. During discharging, it converts the chemical energy into electrical energy and release the stored lithium ions. And it can be repeated for many times. The redox reaction take place at two electrodes, in which the lithium ions intercalate and deintercalated among active materials. The electrons are generated during the process and move through the external circuit to produce current. For keeping electrical neutrality, the lithium ions flow through electrolyte.

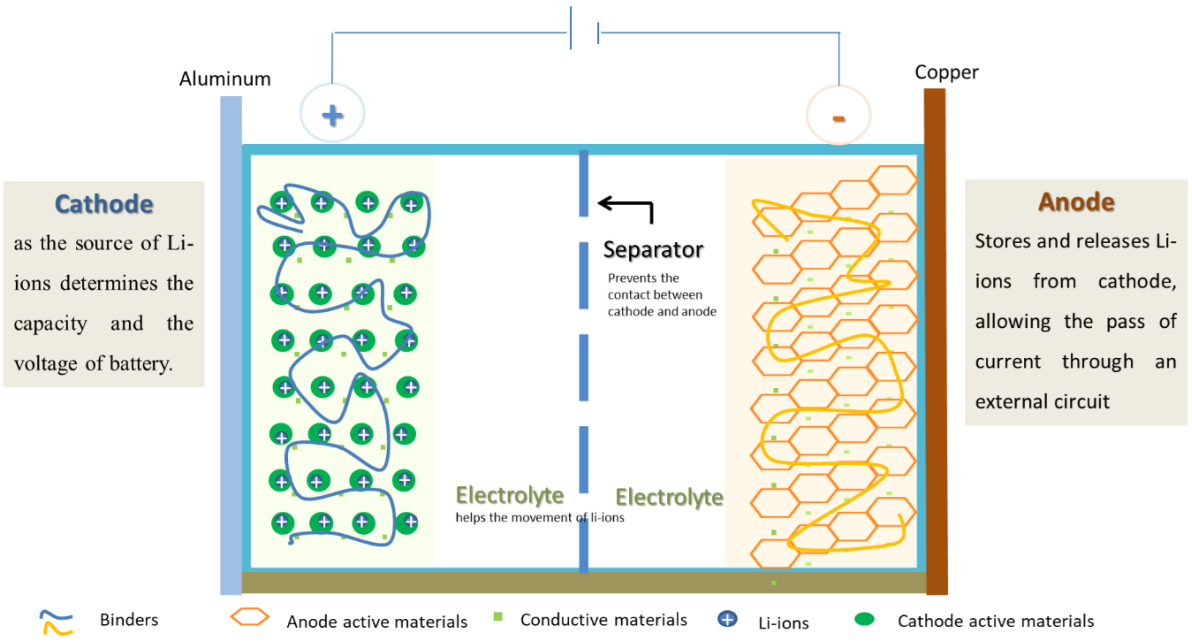

Figure 1-2 the structure of LIBs

1.2 Major components of LIBs

The LIBs contain four main components: cathode, anode, electrolyte and separator. As above mentioned, each component plays a significant role. Therefore, the selection of appropriate materials for each part is critical to optimize LIBs performance. LIBs are expected to produce good electrochemical performances, with stable cycle reversibility, fast ion transfer rates, good conductivity, excellent electrical output, and a long-life span. this section has summarized the influence of active materials, electrolyte, and separators.

1.2.1 Cathode

Cathode is a critical component in LIBs, it determines battery capacity and voltage. multiple categories of cathode have been studied and developed for high-retention discharge capacity, operating voltage, energy and power density etc. each of them possesses advantage and disadvantage.

Figure 1-3 shows three types of cathode materials. $LiMPO_4$ (where M= Fe, Mn, etc) belongs to olivine structure with one dimensional channel for easy diffusion of Li^+ ions during the lithiation and de-lithiation process. due to a lot of advantages like environmental friendliness, abundant, safe, relatively high-capacity retention and low-capacity fading, it attracts considerable attentions in LIBs market. However, its low energy density hindered its application in electrical vehicle industry. Layered transition metal oxide structure like $LiMO_2$ (M= Co, Mn, Ni) as potential cathode materials have continued to be studied and developed due to their high Li^+ ions mobility. The layered structure constructs a two-dimensional Li^+ ion plane which is favorable to ions diffusion and promotes electrical conductivity. $LiCoO_2$, as previously mentioned, paired with graphite anode was the first commercialized secondary battery with an operating voltage of ~4 V. But the materials composed of $LiCoO_2$ are unstable at high temperature and voltage, fast capacity fading at high currents, what's more, the structure of $LiCoO_2$ degrade with time. Based on that, the dope combination of Ni, Mn and Co provide high specific capacity, low resistance,

and stability, respectively. Variety of other layered cathode materials like NCM series has been researched and commonly used in battery market in the past years. Spinel cathode materials like $LiMn_2O_4$ (LMO) with three-dimensional path way. which facile Li^+ ions diffusion. despite the advantages such as good electrical conductivity and high lithium-ions diffusion etc. of LMO, the low energy density and capacity restrict its wide use.

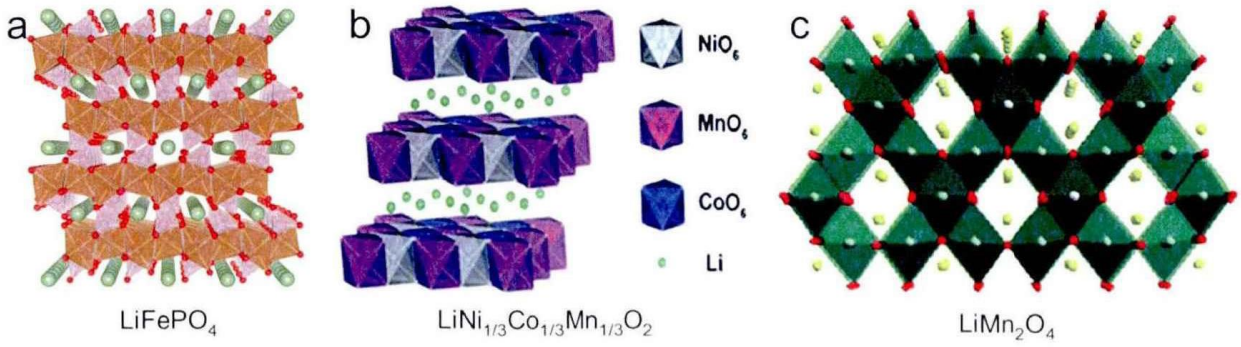

Figure 1-3 the main three different structure of cathode materials

1.2.2 Anode

Anode also plays a significant role in LIBs, it receives and stores the lithium ions from cathode, therefore, the anode materials are expected to possess the following properties: (1) high capacity, (2) low operational voltage platform, (3) good electrical and ionic conductivity, (4) structure stable during lithiation and de-lithiation, (5) forming a stable SEI layer and (6) low cost.

Carbon based anode materials like graphite, soft carbon, and hard carbon were investigated and commercialized in the past decades because of their mechanical, electrochemical and thermal stabilities. Typically, graphite was first commercially used around 30 years ago and even by now, it is still widely used in battery market. During the lithiation and de-lithiation process, as the equation (1-1) shows, 1 Li atom combines with 6 C atom, it causes small volume change (~10%), and exhibits high electrical conductivity and excellent cycle stability. But the theoretical capacity (371 mA h g^{-1}) of graphite could not satisfy the demands nowadays, so many researchers and company has investigated more promising anode materials such as Titanium-oxide-based anode like $Li_4Ti_5O_{12}$ (LTO), alloying materials such as germanium (Ge), silicon (Silicon), tin (Sn), iron (Fe), and cobalt (Co) etc.

$$LiC_6 \leftrightarrow C_6 + Li^+ + e^- \quad (1\text{-}1)$$

Among them, silicon has attracted more attentions in recent years because of its high theoretical capacity (~4200 mAh g^{-1}.), low discharge potential and abundant in earth however, silicon has large volume change (~310%) during changing and discharging process. those problems influence battery overall performance.

1.2.3 Electrolytes

The electrolyte is an essential component in LIBs, the main role of electrolyte is to act as a medium for ions transport between cathode and anode during the charging and discharging process. Thus, the conductive efficiency of electrolyte determines inner resistance of battery. Besides, the electrolyte keeps in close contact with two electrodes and separators. As well-known, the reaction of lithium and water is violent and generate lithium hydroxide and hydrogen. So, the electrolyte of LIBs should be non-aqueous. In addition, it should satisfy the following basic requirements: (1) the electrolyte could not react with contact materials like electrodes materials and separators. (2) it should provide high Li^+ ion conduction between electrodes materials and reduce internal resistance. (3) it should be electrochemically stable without any side reaction. (4) it must ensure electronic insulation to prevent short-circuits. (5) it must have enough electrochemical stability to endure cell's operating voltage. Based on above requirements, three types of electrolytes developed including (1) liquid electrolytes (Li salt in solvents); (2) solid/gel polymer electrolytes (GPEs), and (3) all solid-state electrolytes. Liquid electrolyte is a common and wide used electrolyte in LIBs.it is normally consisted of lithium salt ($LiPF_6$, $LiBF_4$ or $LiClO_4$) and organic solvent mixtures, such as ethylene carbonate (EC), dimethyl carbonate (DMC) and ethyl methyl carbonate (EMC) and according to the different using situation, some other types of organic

solvents are added. However, the organic components in liquid electrolyte are flammable and unstable at high voltage. those unexpected issues pushed the development of gel polymer electrolyte (GPEs), which consist of polymer matrix and lithium salt. Comparing with liquid electrolyte, GPEs have no electrolyte leakage and nonflammability, hinder dendrite growth and improve safety of cells. However, the low ionic conductivities restrict its application by now. for improving the properties, researchers incorporate polymer with inorganic fillers to form a polymer composite. The introduction of inorganic fillers could compensate the low ionic conductivity of polymer electrolyte. the full inorganic solid-state electrolyte is nonflammable and have highly thermal stability compared to liquid solvent and polymer-based electrolyte. But their framework is not stable, and the void between inorganic electrolyte and electrode material increase the internal resistance of battery.

1.2.4 Separators

Currently, the commonly used separators are polyolefin polymers, such as PP, PE and their combinations. Separators used in LIBs is to block the contact of two electrodes which is a safet barrier to prevent electrical short circuit and allow the migration of ions while prevent the flow of electrons. So, the separators in LIBs normally must be electrochemically stable, have good mechanical strength to resist shrinkage, and have sufficient thermal stability during charging and discharging over the operating temperature. what's more, separators have a porous structure to soak

more electrolyte and promote Li^+ ions flow. The thickness of separator should be as thin as possible. The thinner the separator is, the faster the Li^+ ions migrate.

1.3 The electrodes in LIB

The electrodes of LIBs are composed of active materials, conductive agent, and small amounts of binders. And those materials are coated onto a current collector. The active materials have been described in previous section. They are the Li^+ ions reservoir and receptor. The electrical conductivity of many active materials is not enough to satisfy the electrons flow. therefore, conductive materials add to form electrical network. Appropriate number of conductive materials is useful for improving batteries' capacity and life-span. The basic function of binder in LIBs is to interconnect the active materials and conductive agent together, and adhere all electrode materials to the current collectors. the properties of electrodes determine overall battery performance. Therefore, the fabrication process of the electrodes is critical, including the proportion of each component, the thickness control and the selection of solvent.

1.3.1 The development and classification of binders

As described above, the binders in electrodes act as a bridge between electrode materials and current collector. According to the solubility in solvent, the binders are classified into two categories: organic-based (non-aqueous) and water-based (aqueous).

Polyvinylidene fluoride (PVDF) is a typical organic-based binder. Since the first commercially used binder in LIB by Sony, PVDF occupies a dominant position in batteries market. It offers many good properties such as high mechanical strength, thermal resistance and good processability during slurry preparation process. besides, PVDF binder has highly electrochemical stability in a wide potential window (> 5 V vs Li^+/Li). So, even by now, it's still a widely commercialized binder. However, PVDF has some limitations. While it applies to silicon anode, it interacts with the surficial function group of silicon by weak van der Waals forces, which leads to poor cycling performance and rate capability. Specially, it needs to dissolve into toxic solvent (N-Methyl-2-pyrrolidone, NMP), which causes environmental concerns.

Based on that, water-based binder becomes a better choice. Carboxymethyl cellulose (CMC) is a presentative water-based binder. There are many function groups like -OH, -COOH on the backbone, which ensure CMC could interreact with the groups on the active materials surface by hydrogen bond. What's more. CMC derives from cellulose, it's a low-cost and pollution-free materials, importantly, the great dispersibility and compatibility with active materials and conductive materials make it be alternative binder to PVDF. But its intrinsic weakness like brittleness, small elongation rate and stiffness limit its application. So, CMC are not able to suppress and accommodate large volume changes. The cracks and collapse in electrodes might occur. To solve those problems, styrene-butadiene rubber (SBR)

has been synthesized and studied as a binder in LIBs. many reaches reported that SBR could provide stronger adhesive strength, higher flexibility and better mechanical properties. But the viscosity of SBR is too low to coating. The combination of SBR and CMC is a better way to slurry preparation. SBR uses as a binder, CMC acts as thickening agent. However, as the development of binders, they are expected to possess more functions not just a basic binding reagent. the traditional binder whatever PVDF or SBR/CMC, are could not accommodate the isolation resulting from volume expansion. The isolation materials in electrodes would not undergo further lithiation and cause the capacity loss. Thus, the considerable researches work on new water-based binder. Such as Polyacrylic acid (PAA) and its derivatives, Chitosan-based binders, alginate-based binder and so on.

1.4 The methods of polymeric binder synthesis

Binder is micromolecular material which synthesized by condensation and addition polymerization. Condensation polymerization as shown in figure 1-2 extends the polymer chain by function group reaction of bifunctional monomers. Addition polymerization grows up the polymer chain by the repeated addition of monomers which contains at least one double bonds.

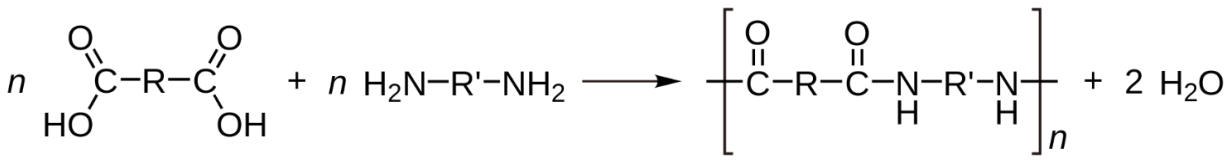

Figure 1-3 schematic diagram of condensation polymerization

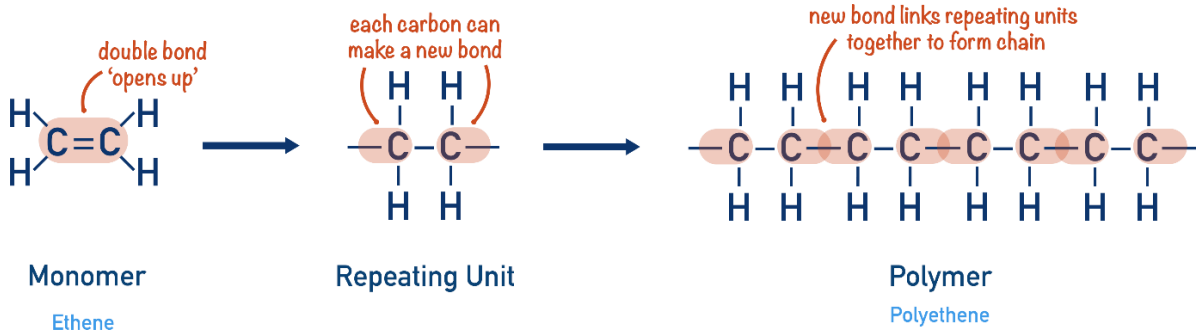

Figure 1-4 schematic diagram of addition polymerization

Free radical polymerization and emulsion polymerization are mechanism and physical methode of addition polymerization for binders' synthesis. The polymer chain grows up through the successive addition of repeat units. During the process the free radicals are formed by variety of mechanisms, usually, the initiators decompose firstly, and then, the free radical adds to monomers, thereby growing the polymer chain. There are many types of initiators, such as thermal decomposition, photolysis, redox reactions, and persulfates etc. In our researches, an aqueous persulfate-type initiators was used.

The emulsion polymerization was firstly explained and developed by Smith and Ewart, and Harkins in the 1949s. the solution for emulsion polymerization, as shown in figure 1-6, has three main components, monomers, initiators and surfactants (emulsifier), surfactant has both hydrophobic and hydrophilic segments, which could make the surfactant disperse into water. When the concentration of surfactant in water exceeds its critical micelle concentration, the excessive emulsifier aggregates together to form micelles. the initiators are present in water phase because the initiators are water-soluble, thus, the radicals also are produced in water. Most monomers are wrapped by surfactants called monomer droplets. Few exist in water and micelles. That is due to the monomers are organic and could not soluble in water. The total surface area of droplets is much smaller than micelles, therefore micelles are more competitive in capturing radicals. It explains that the main site of polymerization take place in micelles. And the mechanism of emulsion polymerization can be divided into three stages. In the first stage, the initiators separate into radicals in water, the radicals enter micelles and react with monomers in micelles, until all micelles turn to monomer-polymer particles. this is Smith-Ewart interval 1. And then the monomers in monomer-polymer particles quickly polymerize and extend the polymer chain. During this stage, the monomer droplets supply monomers to keep the concentration of monomers in monomer-polymer particles, until all monomer droplets in water disappear which means Smith-Ewart

interval 2 finished. due to all droplets has been consumed in interval 2, therefore, in stage 3, the chain grows up by consuming the monomers from monomer-polymer particles. Finaly all monomers turn to polymer.

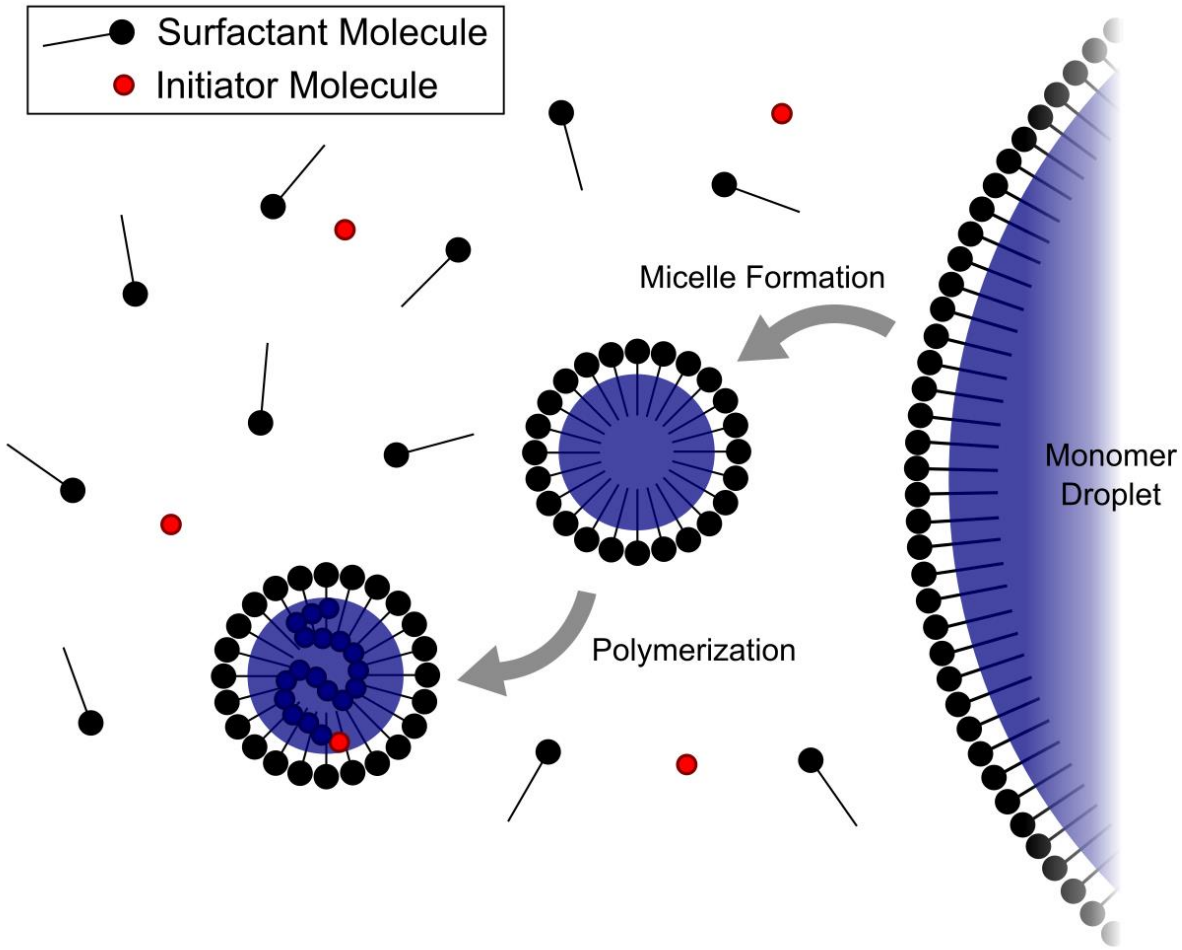

Figure 1-5 schematic diagram of emulsion polymerization

2 Chapter 2 Experimental methods

2.1 Synthesis of binders

2.1.1 Synthesis of MXene clay (Ti2C)-containing in-situ polymerized hollow core-shell composite binder.

The polymerization was conducted in a four-neck round-bottom reactor with a vigorous stirrer, reflux condenser, nitrogen gas inlet system, and feeding devices. The recipes for synthesizing core-shell, hollow core-shell, and MXene/hollow core-shell binders are listed in table as follow:

Components	Seed(g)	Core (g)	Core-shell (g)	Hollow core-shell (g)	Mxene hollow core-shell (g)
MMA	5.5	15	-	-	-
MAA	0.56	12.5	-	-	-
BA	6.5	10	30	-	-
St	-	-	30	-	-
AN	-	-	10	-	-
APS	1	0.2	0.4	-	-
SDBS	0.06	0.05	0.2	-	-
Seed latex	-	50	-	-	-
Core latex	-	-	75	-	-
MXene solution	-	-	-	-	(500mg in seed + 500mg in core process)
Core-shell latex	-	-	-	100	100
5% NaOH	-	-	-	54	54
Distilled water	150	150	150	50	50
Temperature (℃)	75	75	75	75	75

Table 2-1: Recipe of the MC-HCS binder

Seed latex was firstly polymerized to control particle sizes. Multistep emulsion polymerization sequentially was carried out to obtain core and shell polymers in the seed latex. The whole polymerization for CS latex proceeded 5 hours to core

polymers and another 4 hours for shell polymers with 200 rpm stirring at 80 °C under a nitrogen atmosphere. Noteworthy, the core to shell mass ratio was fixed at 1 to 4 to obtain relatively homogenous latex with a regular round shape. HCS binder was completed through the alkalization treatment of the CS latex. The alkalization process was conducted to remove the inner core polymers and to form a hollow core-shell structure. The MC-HCS binder synthesis used the same procedure as the HCS latex. This water-dispersed MCs solution was used in the seeding process instead of pure water. The MCs was first dispersed in distilled water by sonication for 2 h under a nitrogen atmosphere, and then seed monomers were added for subsequent in-situ polymerization on MCs. The exact number of MCs used at the core polymerization step. Fig. 1-1 shows the photographs of the sonicated MCs solution and MC-HCS latex binder, where the binder latex contains 1.67 wt.% of MC.

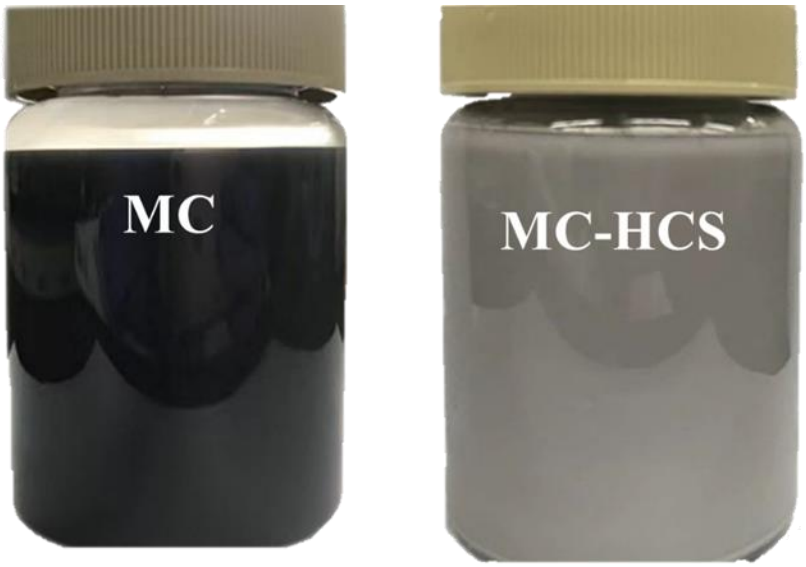

Figure 2-1: The photographs of the sonicated MXene clay solution and polymerized MC-HCS binder latex

2.1.2 Synthesis of tannic acid cross-linked zwitterionic copolymer binder

To prepare zwitterionic copolymer, poly (sulfobetaine methacrylate-co-Acrylamide) (SBAAm), the monomers of Sulfobetaine methacrylate (SBMA) and Acrylamide (AAm) were firstly dissolved into 100 mL deionized water. After the temperature reached 75 °C, 2 wt% of amino-1-propanesulfonic acid (APS) solution as initiator dropwise added into the solution and kept for 1.5 hours. At the same time, poly (vinyl alcohol) (PVA) powder dissolved into 50 mL deionized water and was initiated at 75 °C by APS. Following that, the two solution transferred into one pot and physically mixed for 15 min. And then tannic acid solution dropwise added into

above solution and maintained for 3 hours at 75 °C Finally, tannic acid crosslinked PVA/PSA (TA-c-PVA/SBAAm) binder obtained.

2.2 Slurry and electrodes preparation

2.2.1 Preparation of LiFePO4 (LFP) cathode electrodes

The water-based electrode slurry was composed of 90 wt% of active material LFP (Advanced Lithium Electrochemistry Co. Ltd, Taoyuan City, Taiwan), 5 wt% of super-p (SP, Alfa Aesar, Tewksbury, MA, USA), 2 wt% of thickener CMC (Daicel Fine Chem Ltd., Osaka, Japan), and 3 wt% of water-based binders PAL or SBR (Zeon Corporation, Tokyo, Japan). PAL (Eco chemical Co. Ltd., Ulsan, Korea) is a type of polyacrylate manufactured from emulsion polymerization; due to the policy of the company, the detailed components of the PAL are not available. The organic-based electrode slurry was composed of LFP, SP, and PVdF (90:5:5 wt.%), and NMP was used as solvent. The slurry was mixed in a planetary ball mill and casted on aluminum foil. The water-based and organic-based electrodes were dried in a convection oven at 60 °C and 120 °C for 30 min, respectively. Next, the electrodes were dried again in a vacuum oven at 70 ℃ overnight. The mass loading of electrodes was 11.9 ± 0.4 mg cm ^{2}. Preparation of silicon anode electrodes

2.2.2 Preparation of silicon anode electrodes

The slurry prepared with silicon (Si, 50-60 nm, KCC Co. Ltd.) active material, super-p (SP, PHOENIX) conductive agent, binders, and thickener CMC. The mass

ratio in the slurry was 60:20:10:10 to Si: SP: CMC: binder, respectively. After well mixing in a planetary ball mill (Pulverisette 7, Fritsch), the slurry was coated on copper foil with the doctor-blade method, and dried in a convection oven for 30 min at 60 °C. The mass loading of Si electrodes was 0.7~1 mg cm^{-2}. Before assembling, the electrodes were dried in a vacuum oven at 70 ℃ overnight and fabricated into CR2032 type coin cells in an argon-filled glovebox.

2.2.3 Preparation of silicon/graphite (Si/C) anode electrodes

The preparation of silicon/graphite (Si/C) electrodes is similar with silicon electrodes. Si/C (25 wt%/75 wt%) anode electrodes were prepared as active material, super-p as conductive agent, and binders. The mass ratio of the slurry was 75: 15: 10 to Si: SP: binder, respectively. All the materials were mixed in a planetary ball mill (Pulverisette 7, Fritsch). The well-mixed slurry was coated on copper foil with the doctor-blade method, and dried in a convection oven for 30 min at 60 °C. The mass loading of Si/C electrodes was 1-1.3 mg cm^2. Before assembling, the electrodes were dried in a vacuum oven at 70 °C overnight and fabricated into CR2032 type coin cells in an argon-filled glovebox.

2.3 Cell's fabrication

LFP used as the working electrodes, CR2032 coin-half cells were assembled with polypropylene separator film, a lithium chip as a counter electrode, and 1 M

LiPF6 in 1:1:1 ethylene carbonate: dimethyl carbonate: ethyl methyl carbonate by volume (Panaxetec Co., Busan, Korea) as electrolyte.

In the case of both Si and Si/C electrodes used as working electrodes. A lithium chip (MTI Korea Co. Ltd.) and 1.15M LiPF6 ethylene carbonate/fluoroethylene carbonate/propylene carbonate/diethyl carbonate/ ethyl methyl carbonate (EC: FEC: PC: DEC: EMC=20:10:5:40:25 in volume) (Soulbrain Co., Ltd, Korea) were used as the counter electrode and electrolyte, respectively. A polypropylene separator (Celgard LLC) was placed between the working Si and the counter Li electrodes.

2.4 Physical characteristics

2.4.1 Fourier-transform infrared analysis (FTIR)

ATR-FTIR and FTIR (FTIR, Thermo Scientific Nicolet iS5) used to characterize the functional groups of binder over the wavenumber range, 500–4000 cm^{-1}.

2.4.2 Raman analysis

The Raman spectroscopy (DXR Raman Microscope, Thermo Fisher Scientific) was conducted under λexc = 532 nm laser excitation.

2.4.3 Thermogravimetric analysis (TGA)

The thermal stability of polymeric binder in LIBs was investigated by Thermogravimetric analysis (TGA) under a nitrogen atmosphere and a heating rate

of 10 °C/min, carried out by TA Instruments Q50. The synthesized polymers were dried at 60 ℃ overnight. The polymer film was heated up in a platinum pan from room temperature to 600 °C.

2.4.4 Differential Scanning Calorimetry (DSC)

Differential scanning calorimetry (DSC, TA Instruments Q50) was used to invistage the glass transition temperature (T_g) of the polymers. It was conducted under a nitrogen atmosphere and with a heating/cooling rate of 15 °C/min, and heated from -50 °C to 200 °C.

2.4.5 Zeta potential analysis

The particle size was measured by zeta potential (ZEN3600, Zetasizer Nano ZS, Malvern Instruments Ltd.)

2.4.6 Viscosity tests

The viscosity tests was carried out through Rheometer (HR20, TA-Instruments) under a shear rate ranging in 0.1-1000/s.

2.4.7 Contact angle (CA)

The contact angles of the polymer films are measured by an optical tensiometer (Theta life, Biolin Scientific). It recorded the angle change of one electrolyte droplet on binder films in 60 seconds.

2.4.8 Electrolyte uptake (EU)

The electrolyte uptake of binder films was calculated by adsorption rate in a certain period. The polymer films were dried in a Teflon disc under 40 °C overnight. These fully dried films soaked into electrolyte and recorded the weight change before and after immersed in electrolyte. the EU calculated as the equation below:

$$W_1 = \frac{W_1 - W_2}{W_1} \times 100\% \quad (2\text{-}1)$$

2.4.9 Transmission electron microscopy (TEM)

The Transmission electron microscopy (TEM, JEM-2100F, JEOL, Japan) was used to examine the morphology of binder.

2.4.10 Scanning electron microscope analysis (SEM)

Scanning electron microscope (FE-SEM, JSM-600F, JEOL, Japan) SEM was conducted to observe the morphology of binder and electrodes before and after cycling.

2.4.11 Tensile test

The mechanical properties were studied by a texture analyzer (TA-PLUS, LIoyd Instruments Ltd.). the testing samples were completely dried under 60 °C. and the films were cut into strips with a width of 2 cm and a length of 7 cm. and then tested under tension speed of 10 mm min^{-1}.

2.4.12 Ionic conductivity of polymeric membrane

To calculate the ionic conductivity, electrochemical impedance spectroscopy (EIS, VSP, BioLogic Science Instruments) was implemented at OCV in the frequency range from 10 Hz to 100 kHz using a stainless-steel cell and equation (2-2):

$$\delta_i = \frac{l}{R \times A} \tag{2-2}$$

where δ is the ionic conductivity, l is the thickness of binder film, R is the bulk resistance obtained from EIS, and A is the area of binder film. The electronic conductivity of HCS and MC-HCS were measured using the Wagner-Hebb method.

2.4.13 Adhesion strength

The electrode sheet's adhesion strength was measured through 180° peel force of 2 cm wide strips with a texture analyzer (TA-Plus, Lloyd Instruments Ltd.) at a propagation speed of 60 mm min^{-1}.

2.4.14 Electrical resistance and resistivity

The resistance and resistivity of the electrode sheet investigate using a 46 multipoint probes system (RM2610, Hioki Corp., Japan) at room temperature.

2.5 Electrochemical properties

2.5.1 Galvanostatic charge-discharge test

Long cycling performance of silicon electrodes in a coin cell was examined using the charge/discharge process at 0.1C for the first 2 cycles and 0.5C for the following 100 cycles. Here the capacity of 1C is 4,200 mAh g^{-1}. Cells operates at various current densities for rate efficiency testing from 0.1C to 5C. Both experiments were operated in PNE solution (PEB0501 system, Korea) in a voltage window of 0.005 V to 1.5 V.

In the case of LFP, Long-term cycling and rate capability tests were conducted between 2.5 V and 4.0 V with a CC/CV charge mood and a CC discharge mood. For long-term cycling tests, the cells were charged/discharged at 0.1 C for the first 3 cycles and at 1 C for the next 100 cycles. The cells were charged/discharged with a variety of currents, ranging from 0.1 C to 10 C.

2.5.2 Voltammetry and Impedance analysis

Cyclic voltammetry (CV) and EIS of the cells perform using a potentiostat (VSP, BioLogic Science Instruments). For silicon-based cells, CV scans with a scanning rate of 0.5 mV s^{-1} in the voltage range of 0.0-1.5 V. The EIS was recorded in a frequency range of 0.01 Hz to 100 kHz at 0.2 V vs. Li/Li^+ and with an amplitude voltage of 7 mV.

For LFP, it was performed in the voltage range from 2.0 to 4.5 V, with 10 mV s^{-1} for HS-3E flat cells and 0.25 mV s^{-1} for CR2032 cells using a potentiostat. The electrochemical impedance spectroscopy (EIS) test was performed in the frequency range from 10^{6} Hz to 10^{-2} Hz at the direct current potential of E = 3.5 V.

Electrochemical impedance spectroscopy (EIS) was operated under potentiostatic mode which is fixed with AC amplitude of 10 mV and a frequency range from 100 kHz to 0.01 Hz.

3 Application polyacrylate Latex as binder for high voltage cathode

3.1 Introduction

In recent years, lithium-ion batteries (LIBs) have extended their applications from small portable devices to electric vehicles (EV) and energy storage system(ESS)[4–7]. There are several imperative issues for the LIBs: high energy density, prolonged cycle stability, excellent rate capability, low cost, safety, and environmental-friendly manufacturing process. To cope with the issues, all components of LIB electrodes should be optimized according to their application. The electrodes are normally composed of active materials as a major component, and conducting agent and polymeric binder as minor inactive components[8].

Lithium transition metal oxides such as lithium cobalt oxide, lithium nickel-manganese-cobalt oxide, lithium nickel-cobalt- aluminum oxide have been widely studied in decades[9–14]. However, cobalt and nickel are classified as less-common, carcinogenic, mutagenic, and reprotoxic metals which should be avoid as much as possible in the future LIB manufacture[15,16]. Hence, $LiFePO_4$ (LFP) containing abundant and environmental-friendly iron attracts many researchers' and industries' attention[17–22]. LFP is also known for its high thermal stability with appreciable capacity (170 mAh g^{-1}) and excellent long-term cycle stability[23].

Apart from the active materials, polymeric binder is also an indispensable element in LIBs that play a crucial role in maintaining electrical network integrity of the electrode, though it is inactive to electrochemical reactions[24–27]. As a conventional binder for the cathode, polyvinylidene fluoride (PVdF) has been normally used due to its good chemical and electrochemical stability[28–30]. However, PVdF should be used in the form of solution with toxic and flammable organic solvent, N-methyl pyrrolidone (NMP) during the preparation of electrode slurry[31–33]. This certainly issues the difficulty in manufacturing of electrode and increases the cost of manufacturing[34]. Therefore, there have been intensive studies on water-based binder, such as styrene-butadiene rubber (SBR), carboxymethyl cellulose (CMC), sodium alginate, polyacrylic acid, Polyvinylpyrrolidone, etc[35–39]. Among them, SBR is known as one of the most common water-based binders

because of its good flexibility, strong binding force, and high heat resistance[40,41]. Especially, SBR combined with CMC is widely applied for commercial graphite anodes[41–43]. However, SBR is oxidized when the voltage over 4.2 V is applied to $LiCoO_2$ cathodes, because unsaturated C=C double bonds in the polymerized butadiene chains of SBR are unstable such a high voltage[44]. This is one of the reasons to limit the implement of water-based SBR binder on LIB cathodes.

Polymeric binder as an inactive component should be stable in anodic and cathodic environments. This is essential to exploit a potential water-based binder that has good electrochemical stability in a wide voltage window when applied to LIB cathode. In this study, a new water-based polyacrylate latex (PAL) binder will be applied to commercial LFP cathodes, and compared to typical SBR and PVdF binders with their electrochemical stability. Besides, the comprehensive electrochemical tests of LFP cathodes produced by the new binder or the two typical binders will be performed and discussed carefully.

3.2 Results and discussion

3.2.1 Electrochemical characterization

First of all, the electrochemical stability of the binder is investigated through CV of HS-3E flat cells and the result is shown in Fig. 3-1. During the 3 cycles within 2.0~4.5 V, the oxidation peaks appear at voltages approximately above 4.2 V only in the SBR electrode, although the peak intensity decreases as the cycle proceeds.

However, there is no corresponding reduction peak in the cathodic scan to 2.0 V, indicating that the oxidation of SBR is irreversible. This is consistent with the previous study. Yabuuchi et. al[45] reported that the unsaturated C=C of butadiene chains in SBR was oxidized at higher than 4.2 V. In contrast, no distinguishable oxidation peaks exist in the CV curves of PAL and PVdF electrodes other than typical electrochemical double layer characters[46]. Therefore, there is no doubt that the PAL is electrochemically as stable as PVdF within the cathodic working voltage. The slight current increase of PAL and PVdF electrodes during anodic scan nearby 4.5 V is attributable to the electrochemical decomposition of electrolyte. From this simple CV result, the new water-based PAL can be applied as a cathodic binder, at least over LFP electrodes, unlike to SBR binder.

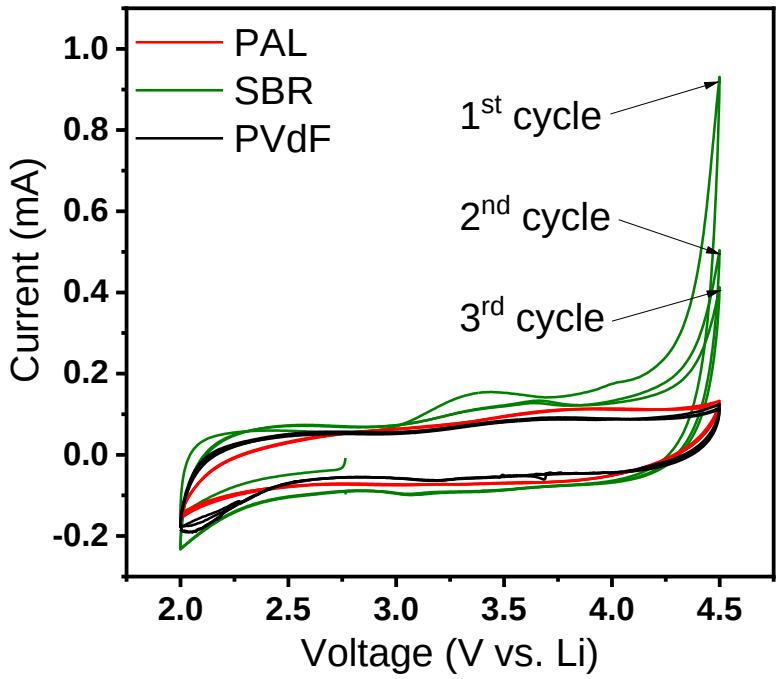

Figure. 3-1. Cyclic voltammetry of the binder electrodes. The binder electrodes are composed of SBR, PAL, or PVdF with excess amount of SP conducting agent.

In addition to an environmental-friendly character of water-based latex binders, another outstanding benefit of the latex binders is the use of smaller amount binder compared to typical organic-soluble PVdF binder. Because the binder is an electrochemically inactive component of electrodes, its content should be minimized in electrode if possible. Unlike the PVdF binder of surface contact mechanism, water-based emulsified binder such as SBR or PAL contacts the active material by

point-to-point binding mechanism with its fine polymer particles [47].The fine particles of water-based emulsified binder can help to keep electrode integrity with less amount than PVdF, ultimately leading to an increase in capacity and rate capability, although it is still ambiguous how small particles are best for LIB electrodes. As shown in Fig. 3-2, the average size of PAL particles is around 182 nm whereas that of SBR particles is approximately 104 nm. The particle size can be easily controlled by modifying the emulsion polymerization techniques and components, and is out of our scope for this study.

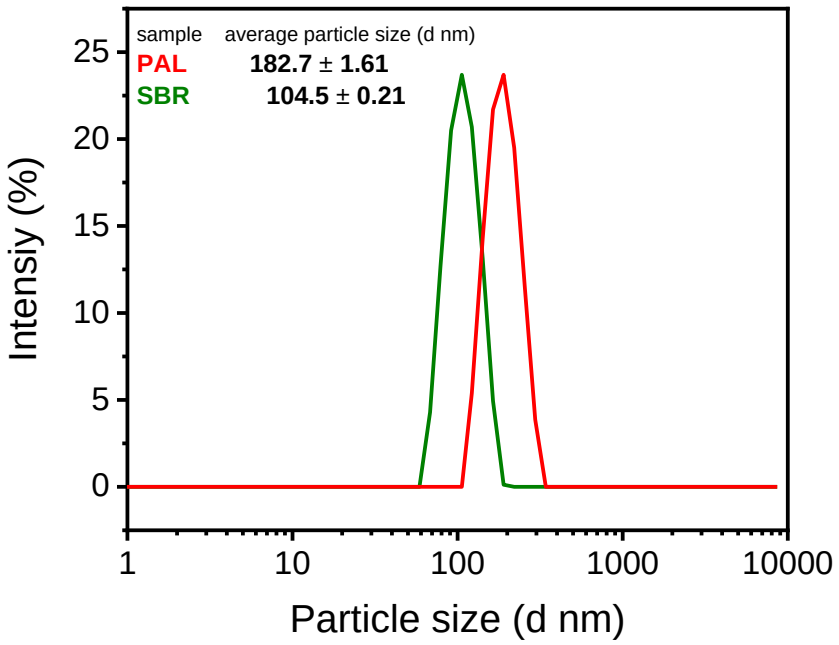

Figure. 3-2. Particle size distribution of PAL and SBR latices.

The most important properties of electrodes in terms of binder are the adhesion and the electrical resistance of the electrodes. The electrode adhesion is first examined via a mechanical peel test of the electrode from the current collector and the result is shown in Fig. 3-3(a). No meaningful peel strength was observed for the LFP electrode containing PVdF binder. Meanwhile, the LFP electrodes containing emulsified PAL and SBR binders are approximately 15.8 N cm^{-1} and 25.1 N cm^{-1}, respectively. As displayed in Fig. 3-3(a), however, the peel strength of the LFP/SBR electrode is not as stable as that of the LFP/PAL electrode during the test. This implies that the PAL binder disperses in electrode better than the SBR binder does. This is also confirmed by the pictures in Fig. 3-3(b) that show the dispersion of SP in the binder latices. Due to the hydrophobic nature of carbonaceous SP, SP is hardly dispersed in water. Compared to the dispersion of SP in SBR latex, SP is relatively well dispersed in the PAL latex. This must be attributed to the functional groups in acrylate such as carboxylate, which can easily interact with the functional groups on the surface of SP as impurities. The uniform dispersion of binder can avoid the aggregation of the active material and conducting agent, which has an advantage for better electrochemical performance of electrodes.

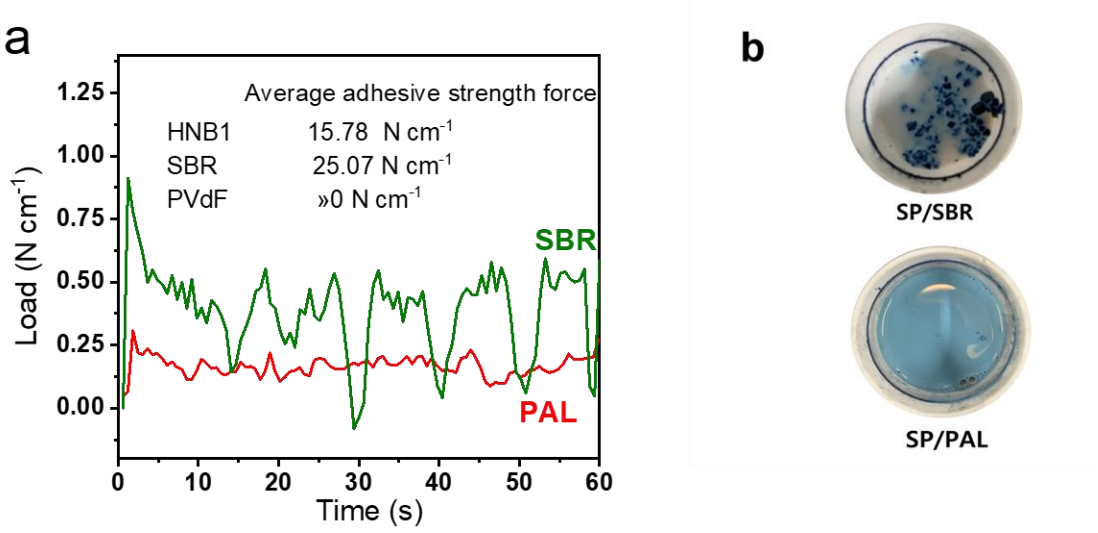

Figure. 3-3. (a) 180° peel strength of LFP electrodes containing PAL, SBR or PVdF binder. (b) Dispersion of SP in PAL and SBR latices.

The electrode resistances are measured using 46 multipoint probes connected to a measurement system. The system allows to measure the electrical resistances of electrode without considering the geometric correction factors caused by typical four-point probes systems. As listed in Table 3-1, the LFP/PAL electrode has the smallest surface and volume resistivities of the three LFP electrodes and has a little higher interface resistance than the LFP/SBR electrode. In particular, compared to commercial PVdF binder, the PAL binder decreases the volume resistivity of the LFP electrode from 12.2 to 7.27 Ω cm, which corresponds to 40.4%. Though a relative lower adhesion of the LFP/PAL leads to a slightly larger resistance assigned to the

interface between the electrode and the current collector than the LFP/SBR electrode, there is no doubt that PAL binder is favorable for producing a LFP electrode possessing lower electrical resistances due to its well dispersion in the electrode.

	Composite thickness (μm)	Composite surface resistivity (Ohm cm^2)	Interface resistance (Ohm cm^2)	Composite volume resistivity (Ohm cm)
PAL	16.4	$1.19*10^{-2}$	2.93	7.27
SBR	16.9	$1.85*10^{-2}$	1.85	7.59
PVdF	18.5	$2.75*10^{-2}$	8.91	12.20

Table 3-1. Surface and volume resistivities and interface resistance of the LFP electrodes.

The electrochemical characteristics of the LFP electrodes were examined using CV and EIS experiments, which are depicted in Fig. 3-4. The LFP electrodes containing PAL or SBR binder exhibit clear and strong anodic peaks at 3.5 V and their symmetrical cathodic peaks at 3.3 V. These are assigned to the oxidation of Fe^{2+} and reduction of Fe^{3+} in LFP, respectively. Regardless of the two binders, the potential gaps of the peaks are almost the same and are nearly 200 mV. One the contrary, the redox peaks of the LFP/PVdF electrode are relatively sluggish and their potential gap is approximately 800 mV, much larger than the LFP/PAL and LFP/SBR

electrodes. It implies that the polarization resistance of the LFP electrode becomes decreased when water-based PAL or SBR binder is used instead of commercial PVdF binder. This may be the reason that the point-to-point contact of PAL and SBR provides more free paths for lithium ions movement in the LFP electrode. Further evidence on this point is given by EIS analysis of the electrodes cycled by four times. These are shown in Fig.3-4(b). The size of the semicircle in the middle frequency range represents the charge transfer resistance for electrochemical reactions occurring at the interface between the electrode and electrolyte [48]. On the contrary, the straight line at low frequency region gives information on the Warburg resistance associated with ion diffusion in the electrode [47]. It is very obvious from the figure that the charge transfer resistances of the LFP composed of PAL (18.4 Ω) and SBR (21.5 Ω) latex binders are much smaller than that of PVdF binder (457.5 Ω). Additionally, the PAL electrode has a steeper slope than the SBR electrode at low frequency, demonstrating a faster ion diffusion in the PAL electrode. Overall, the reduced charge transfer resistance and improved ion diffusion by the use of PAL binder may affect affirmatively the electrochemical performance of the LFP electrode.

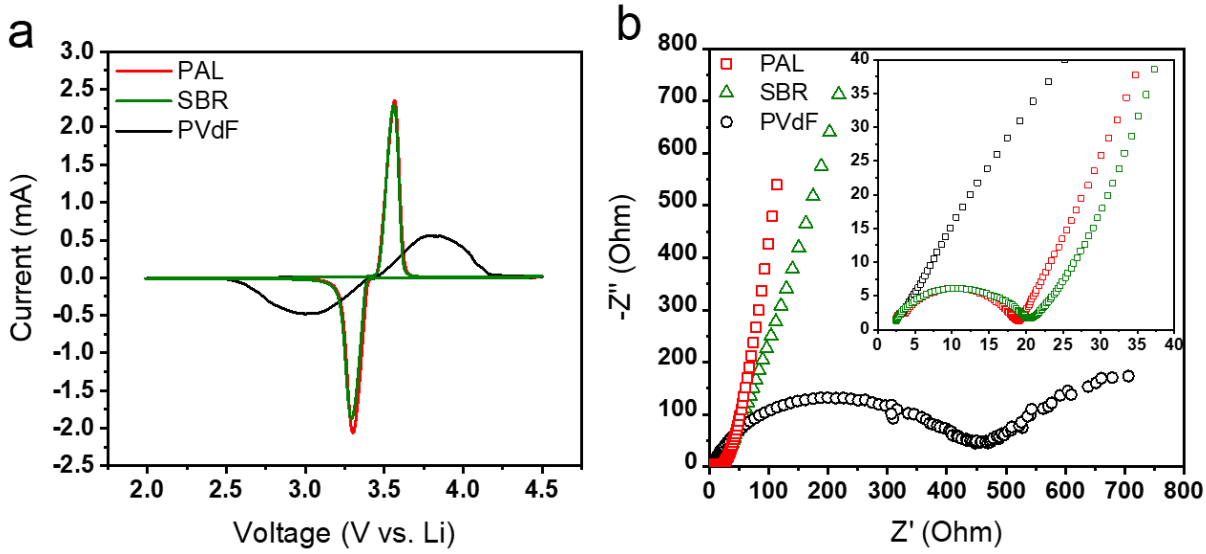

Figure. 3-4. (a) CV and (b) EIS of the LFP electrodes containing different binders.

Finally in Fig. 3-5, the electrochemical performance of the LFP electrodes manufactured by different binders is shown with respect to long-term cycle and rate-capability. The electrodes containing PAL or SBR binder show excellent long-term cycling stability with the specific discharge capacities of 142 mAh g^{-1} for the LFP/PAL and 136 mAh g^{-1} for the LFP/SBR, respectively, after 100 cycles. On the contrary, the LFP/PVdF electrode suffers from severe capacity fading so that the capacity retention is only 7.1% at the 100^{th} cycle. Besides, the PVdF electrode shows serious unstable coulombic efficiency, whereas the others have superior stable coulombic efficiencies above 96%. This is in accord with the results of high-rate capability tests in which the cells are charged and discharged at various current

densities: 0.1C, 0.2C, 0.5C, 1C, 2C, 5C, and 10C. At each current, 8 cycles are repeated and then the current goes back to 0.1C to check the electrode recovery. As shown in Fig. 3-5(b), the PVdF electrode shows low capacities at even low currents of 0.1C and 0.2C, and nearly zero capacity above 0.5C. This might be caused by the network bonding mechanism of the PVdF binder, i.e., weak adhesion strength, high electrical resistances, and significant charge transfer resistance caused by the PVdF binder. In contrast, the PAL and SBR electrodes show good rate performance with relatively higher capacity retention than 50% at even 10C. Additionally, the electrodes fully restore their capacities when 0.1C is given to the electrodes from 10C, implying that there occurs no physical damage in the electrodes for such high current charge/discharge cycles. Furthermore, it is clear from Fig. 3-5(c-d) of the charge-discharge profiles at different current densities that the LFP/PAL electrode exhibits more stable voltage profiles than the LFP/SBR electrode.

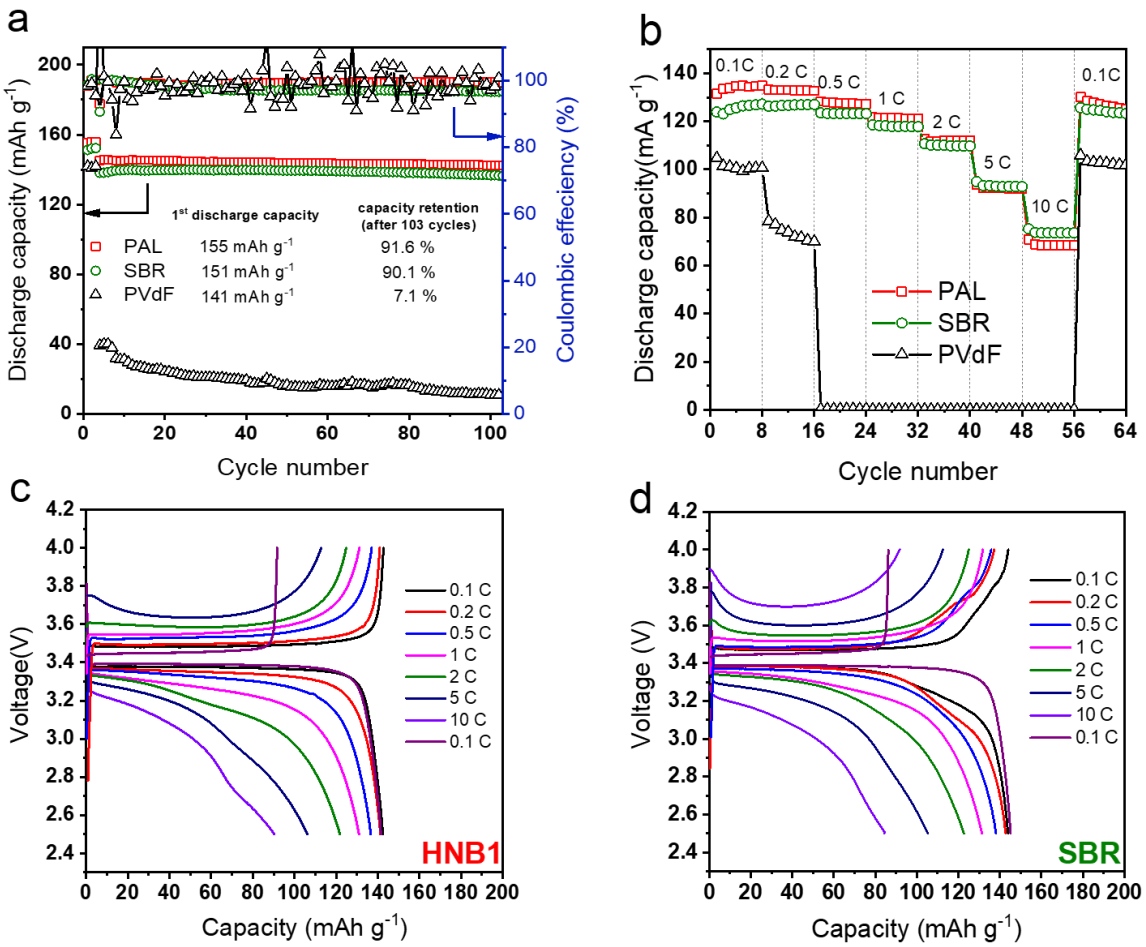

Figure.3-5. The electrochemical performance of the electrodes containing different binders: (a) long-term cycling, (b) rate capability. (c) and (d) are charge and discharge profiles of the electrodes at a variety of current densities.

In summary, the PAL binder is a promising water-based binder candidate for a LFP cathode due to its excellent electrochemical stability at high voltage, pleasant

dispersion in slurry, satisfactory adhesive strength, and small surface and volume resistance.

3.3 Conclusion

Similar to commercial SBR binder for LIB anodes, the new PAL binder makes the manufacturing process of LIB cathodes eco-friendly because it is dispersed in water as an emulsion state. Unlike the SBR binder, more importantly, the PAL binder is unrestrained to expose at such a high working voltage of LIB cathode due to no presence of carbon-carbon double bond in the main chain of PAL. From the CV result, it is confirmed that the PAL has good electrochemical stability up to 4.5 V just like organic-based PVdF binder. Additionally, there are several advantages originated from the point-to-point bonding mechanism of the PAL binder, when compared to the PVdF binder used for normal cathodes. The LFP cathode manufactured by the PAL binder has stronger adhesion strength, lower electrical resistances, and better charge transfer characteristic than that manufactured by the PVdF binder. Consequently, the LFP cathode containing the PAL binder could achieve an excellent specific discharge capacity 155 mAh g^{-1} with high-capacity retention of 91.5% after 100 cycles at 1C. Even the specific discharge capacity remains more than 50% when the charge/discharge current density increases up to 10C. These are much better than the LFP cathode composed of the conventional PVdF binder.

4 MXene clay (Ti2C)-containing in-situ polymerized hollow core-shell composite binder

4.1 Introduction

Silicon (Si) as an anode material has attracted significant attentions due to its advantages of high theoretical capacity (~4200 mAh/g), low operation potential (< 0.5 V *vs*. Li/Li^+), and abundant resources[49]. However, Si anodes suffer from severe capacity fading during the lithiation/de-lithiation process, resulting from Si's massive volumetric expansion (~300%). The repetitive volumetric change of Si worsens the particle-to-particle contacts, leading to the electrical and ionic isolation of Si electrodes and the delamination of the electrode from the current collector [50]. Furthermore, the enormous volumetric expansion results in cracks in the solid electrolyte interphase (SEI) and causes the additional SEI layer growth on the surface of Si [51]. These undesirable phenomena have hindered its application in the energy storage field. In order to alleviate the irreversible expansion and shrinkage of silicon, tremendous researches has been conducted on silicon structure design [52–54], electrolyte modification [55–57] and multifunctional binder study [58–60]. Binder gives an alternative option that can effectively suppress the problems due to its facile fabrication process and low cost.

The fundamental role of a binder in an electrode is to maintain the conductive network of the electrode through the cohesion of the electrode components (e.g., active material and conductive agent) and their adhesion to the current collector during cell operation [61]. Thus, the binder plays a significant role in the mechanical stability of electrodes and their long-term cycling performance. Organic-based polyvinylidene fluoride (PVdF) has been commercially used in LIBs. However, silicon interacts with the surface by weak van der Waals forces, leading to poor cycling performance and rate capability. Additionally, PVdF is dissolved only in a toxic organic solvent (e.g.,N-Methyl-2-pyrrolidone, NMP), which causes environmental concerns during slurry preparation. Although commercial styrene-butadiene latex (SBL) is a water-dispersed binder, its use is limited due to its worse effect of suppressing silicon expansion and maintaining electrical paths when used in silicon- based electrodes. Above all, apart from better adhesion and environmental friendliness, the binders in silicon-based anodes are expected to have better functions to address silicon particles considerable expansion and electrical isolation. Various efforts are emerging, such as self-healing polymeric binders to alleviate expansion and repair electrical network, grafted binders containing electrical and ionic conduction segments to improve conductivity, as well as multifunctional binders to enhance the comprehensive capability [60,62–64].

Two-dimension (2D) materials have recently been widely used in energy storage due to their electronic conduction and good mechanical properties. MXene, as a novel 2D nanomaterial, has attracted significant attention and has been applied in a variety of industries, such as catalysis [65,66], wearable sensors [67,68], and energy storage [69,70] since it was first discovered in 2011[71]. Compared with 2D graphene materials, MXene is more hydrophilic and holds wealthy functional groups (e.g., -O, -F, and -OH) on its surface[72]. These outstanding properties make MXene implementable in water and allow some reactions and interactions with other functional groups (e.g., -OH, -COOH, or -CN)[73]. Many researchers reported MXene/polymer composites such as MXene with polyethylene oxide (PEO)[74], polyvinyl alcohol (PVA) [75,76] polyacrylamide (PAAm)[68] etc. The MXene interacts with polymers by hydrogen bonding force, van der Waals attraction, and electrostatic interaction [77–79]. Combining MXene with polymers can enhance the properties and performances of the composites, including mechanical properties, solution stability, and especially electrical conductivity [80].

Inspired by the conception, we introduce conductive MXene to water-based polymerization and obtain water-based MXene/polymer composite binder to compensate for the shortage of water-based binder without electrical conductivity. Primarily, a water-based binder with a unique hollow core-shell structure was synthesized on the surface of MXene by in-situ emulsion polymerization. Removing

core polymeric components from core-shell structured polymers achieved the hollow core-shell structure. Its empty inside allows Li-ions to shuttle during the charge/discharge process. The removed cores also help electrode slurry to maintain high viscosity in the electrode coating process.

On the other hand, the outer shell design has essential binder properties such as adhesion and mechanical strength, composed of poly (acrylonitrile-butyl acrylate-styrene). The -CN groups in acrylonitrile (AN) provide good adhesion in electrodes, the styrene (St) is typically used to improve mechanical strength [81], and the butyl acrylate (BA) imparts a flexible behavior for the binder to tolerate the deformation during cell operation [82]. The commercial water dispersed SBL binder use as a reference binder. The structure of MXene clay/hollow core-shell composite binder (abbreviated as MC-HCS) confirmed by TEM and SEM spectroscopies, and its physical and electrochemical characterization is examined through various methods.

4.2 Results and discussions

4.2.1 Confirmation of polymerization

Fig.4-1 (a) shows a schematic synthesis of the MC-HCS binder. We first synthesized a core-shell structure on the MXene surface by in-situ polymerization. Later, inner core polymers dissolve through alkalization treatment to obtain a hollow core-shell structure. During the alkalization process as shown in Fig.4-1 (b), the hydroxyl anion (OH^-) from sodium hydroxide is easier to penetrate through the outer shell when the temperature is over glass transition temperature (T_g), and then reacts with a carboxyl group (COOH) in the core polymer [83]. After the alkalization treatment, the core polymers come out of the core-shell structure and finally dissolve in the aqueous medium. Because the T_g of CS (measured by DSC in Figure 4-2) was 13.8 °C, the alkalization conducts at 70 °C, which is significantly higher than the T_g of CS polymer and it is easier for OH^- to transport inside of the shell.

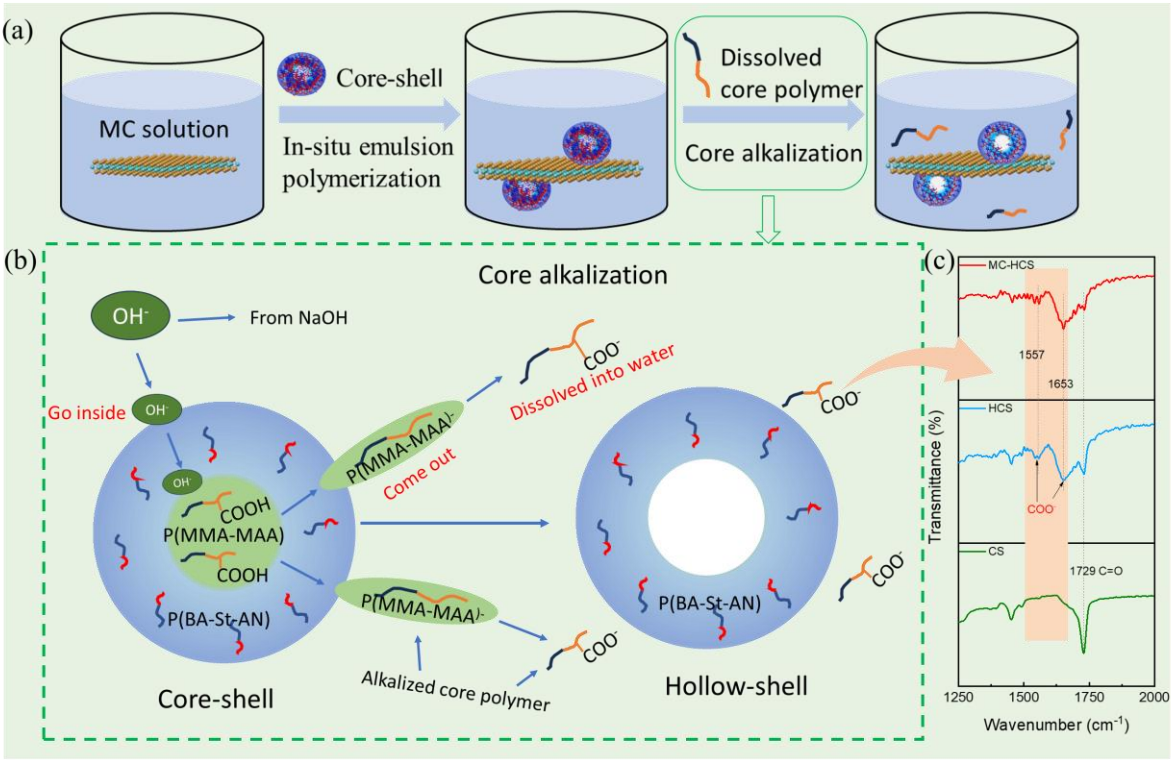

Figure. 4-1. Synthesis process of in-situ polymerized MC-HCS binder (a) schematic synthesis and (b) alkalization process, and (c) FT-IR spectra.

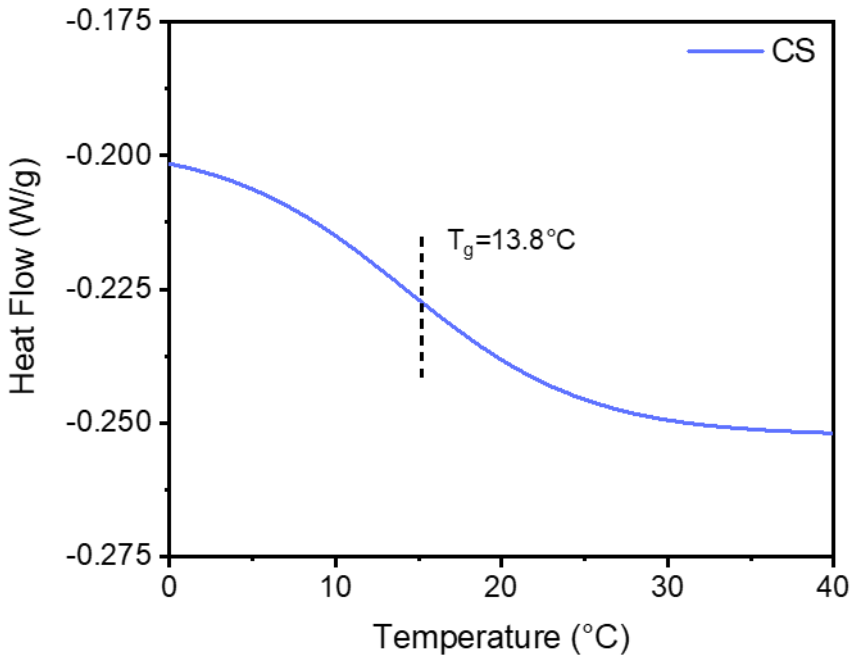

Figure. 4-2. Differential scanning calorimetry thermograms of CS polymer solid film

FTIR and Raman spectroscopy were performed to confirm the successful in-situ polymerization and are shown in Figure. 4-1 (c) and Figure. 4-3. The peak observed at 1452 cm^{-1} is associated with the phenyl C_6H_6 stretching vibration of St [81], and there is also a weak vibration peak at 2276 cm^{-1} contributing to the CN group[84]. The vibration at 1162 cm^{-1} has been attributed to the C–O in R–COO–R of MMA and BA. The intensively strong peak at 1729 cm^{-1} belongs to C=O of BA and MMA, and in the case of CS latex, it also belongs to COOH in MAA of the core polymer [85]. The peak related to COO^- in dissolved core polymer P(MMA-BA-

MAA)$^-$ can be observed at 1557 cm^{-1} [86]. On the other hand, the COO$^-$ vibration influences the presence of the two C=O peaks at 1653 cm^{-1} and 1729 cm^{-1} respectively. The COO$^-$ groups only exist in the HCS and MC-HCS binder. The shift of -COOH to COO$^-$ implies that the inner core polymer was successfully alkalized. The Raman shift in Fig. 4-3 (b) shows that the vibrations of Ti–O, C–Ti and C–F of MCs observes only in the MC-HCS binder.

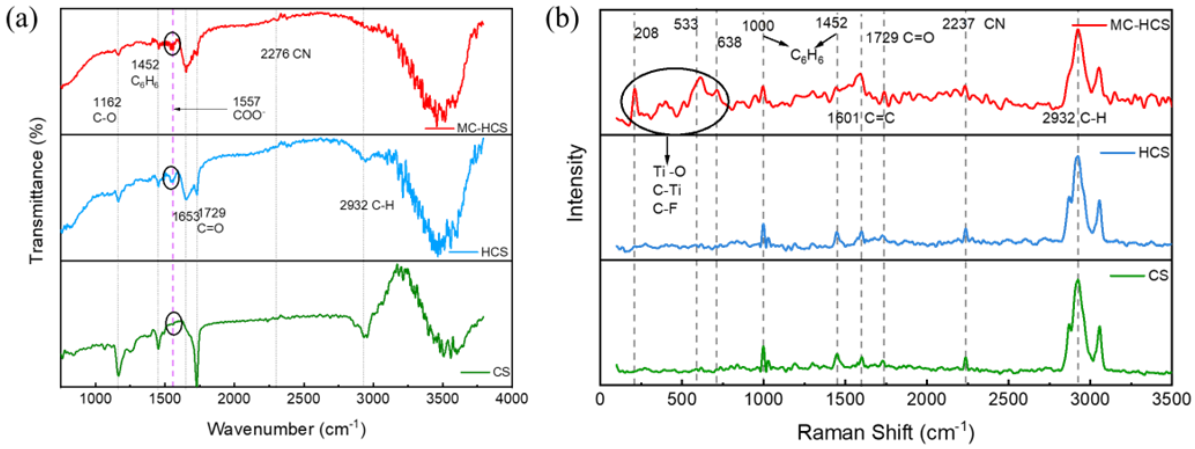

Figure. 4-3. (a) The FTIR and (b) Raman spectrocopy of CS, HCS and MC-HCS binder.

Moreover, the viscosity of HCS and MC-HCS latex shown in Fig. 4-4 is more significant than CS binder latex, proving that the core polymers have dissolved into water after alkalization, increasing viscosity. SEM and TEM further investigated the morphologies of CS, HCS, and MC-HCS.

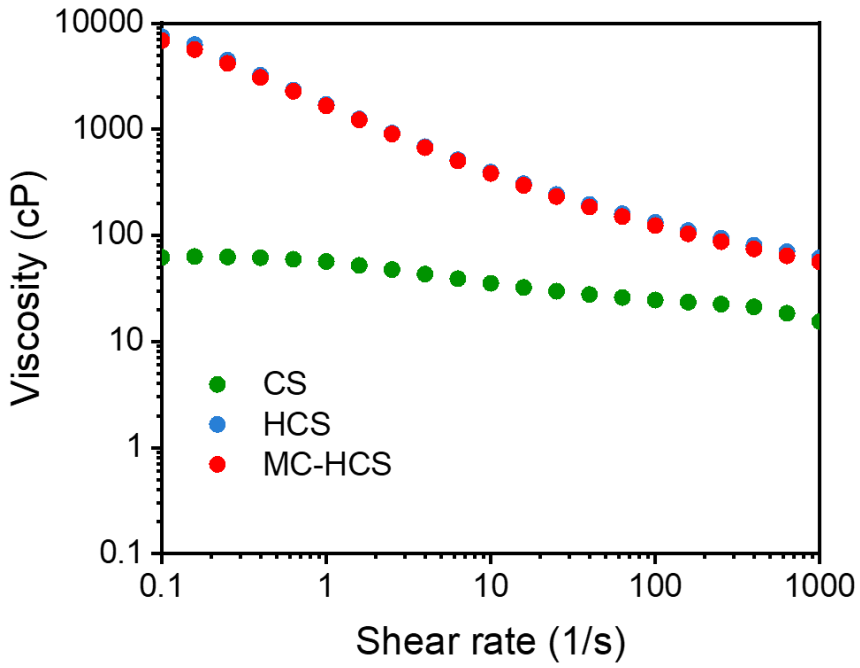

Figure. 4-4. Dynamic viscosity of CS, HCS and MC-HCS latex.

FE-SEM images shown in Figure. 4-5 (a–d) indicate that the particles of CS and HCS binder have a spherical structure, and MCs have a multi-storey structure. Figure. 4-5 (d) shows polymer particles in situ polymerized on the surface of the MCs. More definite morphologies of CS and HCS observes using FE-TEM. Figure. 4-5 (e) demonstrates the structure of the CS binder in that light outer shells wrap the dark inner core part. Figure. 4-5 (f), however, the inner cores of the HCS exhibit lighter when compared to that of the CS particle. This explains that the empty core structure of HCS forms successfully with the alkalization process.

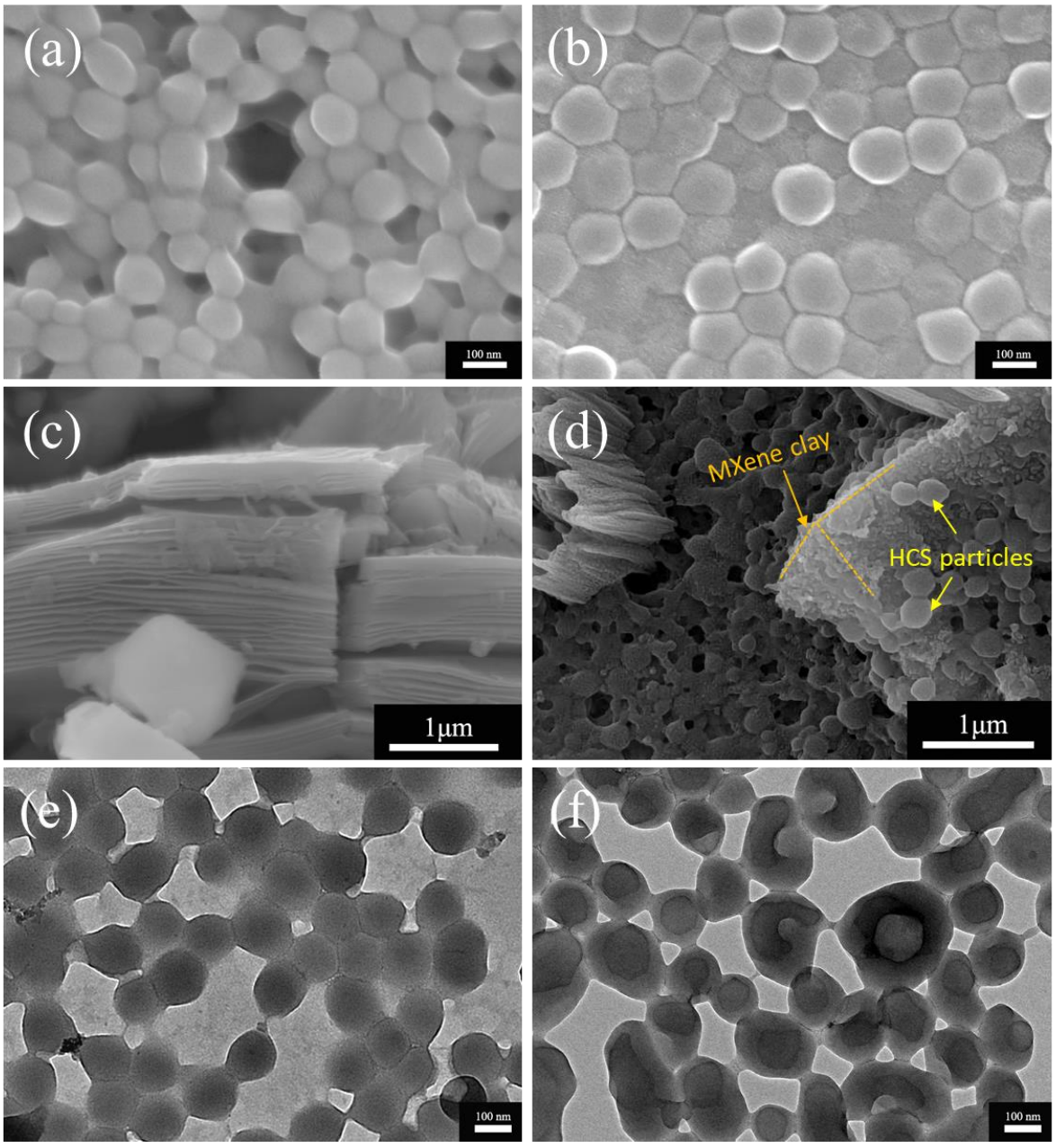

Fig.4-5. FE-SEM images of (a) CS particles, (b) HCS particles, (c) MC, and (d) MC-HCS binder. FE-TEM images of (e) CS and (f) HCS particles.

4.2.2 Physical characterization and electrodes

The wettability and swelling of the binder film in organic electrolyte were examined through contact angle (CA) and electrolyte uptake. And the results were shown in Fig. 4-6 (a) and (b), respectively. Consistently, the hollow core-shell samples, HCS and MC-HCS, show lower electrolyte uptake below 9% (7.1% and 8.9%, respectively) in 4 h, which is close to conventional SBR binder and is much smaller than the core-shell CS binder of 56.4%. The CS binder film suffers such a high electrolyte uptake because the hydrophobic segments in the core polymer of the binder quickly absorb the organic electrolyte solution [87]. As already known, relatively high electrolyte uptake can improve the interface compatibility between electrode and electrolyte. In contrast, massive electrolyte uptake also decreases the interaction capability between binder and other electrode components by the softening and solvation of binder [88,89]. Besides, an abundance of electrolyte solution in electrodes deteriorates the ionic and electric conductions caused by excess electrolyte penetration [90]. Therefore, the relatively small electrolyte uptake of the HCS and MC-HCS binders can ensure good affinity to the electrolyte and structural integrity of the electrode.

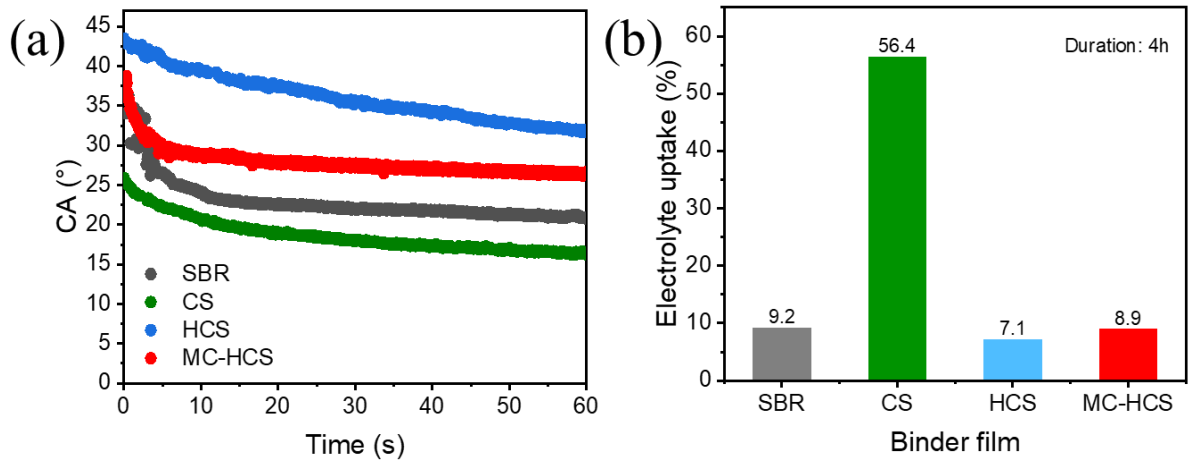

Figure. 4-6. (a) The electrolyte contact angle change in 60 seconds, (b) the electrolyte uptake for 4 h

To examine the effect of hollow core-shell on lithium ions transport, AC impedance was performed by sandwiching the polymer film between two stainless steel electrodes. Fig. 4-7 (a) shows its results. The bulk resistances were obtained from the spike-like lines on the real axis in the Nyquist plot using the equivalent circuit inserted in the figure [91–94]. As presented in figure. 4-7 (b), the ionic conductivities of HCS and MC-HCS calculated from the bulk resistances are 44.3 μS cm^{-1} and 55.8 μS cm^{-1} at room temperature, which are much larger than the CS biner of 6.9 μS cm^{-1} and the SBR binder of 5.9 μS cm^{-1}. This indicates that the hollow core is an efficient binder structure facilitating lithium-ion transport compared with the compact core structure of the CS binder.

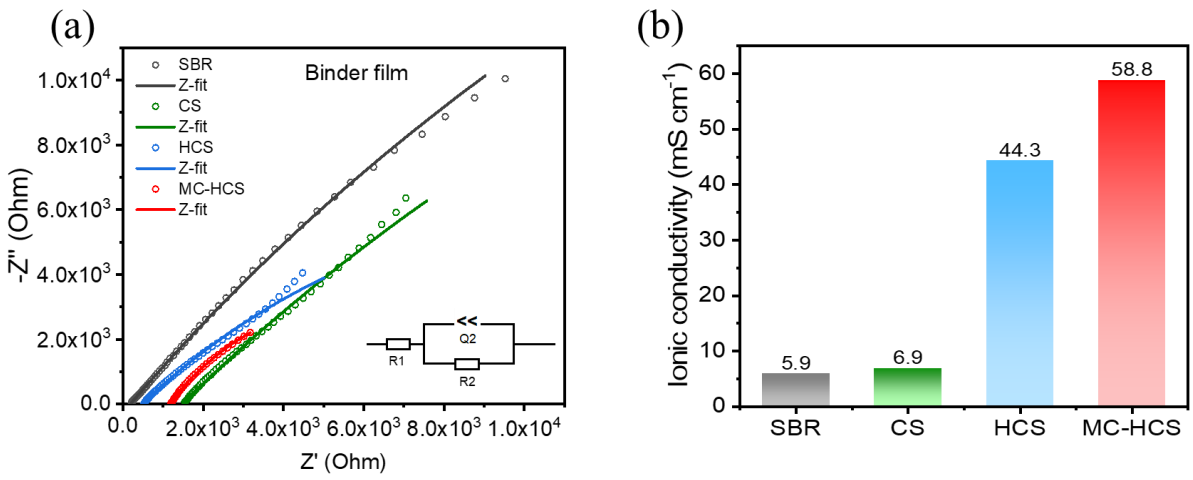

Figure 4-7. (a)The Nyquist plot of the polymer film sandwiched by two stainless steel electrodes. (b) The ionic conductivity.

Before the hollow core-shell samples were finally applied as binder for Si anodes, their thermal stabilities were investigated through TGA because the materials are exposing to high temperatures during electrode drying. Fig. 4-8 shows the experiment results of an exhibit that the HCS and MC-HCS binder films begin to decompose at approximately 340 °C. Though their decomposition occurs early than the CS polymer film of 380 °C, the decomposition temperatures of the HCS and MC-HCS are high enough compared to the electrode drying temperature, so they are thermally stable as the binder for the Si electrodes.

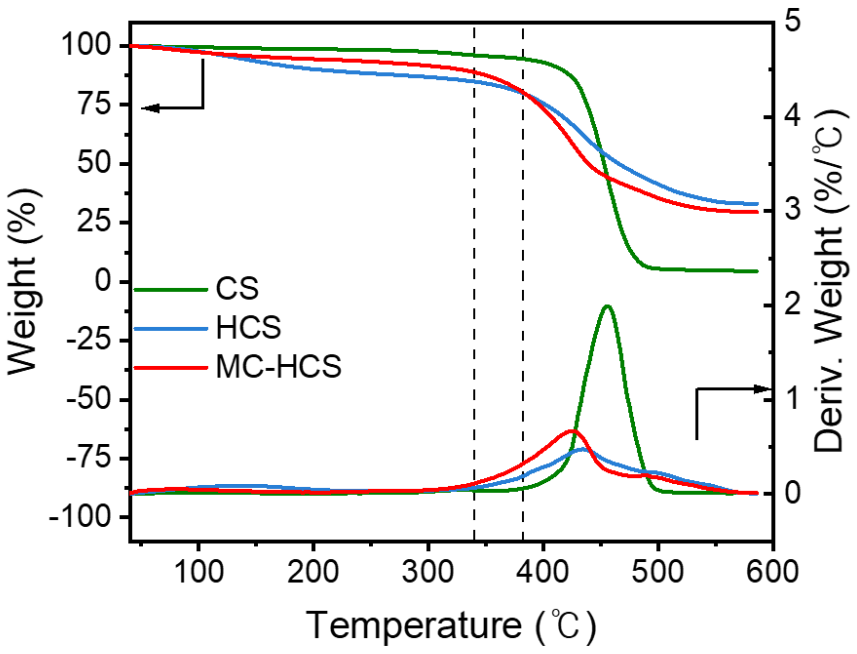

Figure 4-8. The thermogravimetric analysis of CS, HCS and MC-HCS.

The intrinsic huddle of the high-capacity Si anodes is that the volumetric expansion and contraction of the Si particles reaches 310% during lithium ions insertion and desertion, leading to the electrical isolation of the electrode. Therefore, the adhesion ability and resistance of Si electrodes are key factors determining the electrochemical behavior of the high-capacity anode during cell operation. Figure. 3-9 (a) shows the results of the adhesion ability of electrodes with different binders to examinations. The average adhesion strengths of the electrodes fabricated by the SBR and CS binders are lower than 0.5 N, whereas the Si electrodes composed of the HCS and MC-HCS binder show higher adhesive strengths of 0.952 N and 0.692

N, respectively. As shown in Figure. 4-1 and mentioned, the core polymer coming out and dissolved into a binder solution during the alkalization treatment possesses highly adhesive carboxy anions (COO^-) functional groups. This could improve the adhesion strength of the Si electrode. However, the decrease in the adhesion of the MXene-containing HCS is inevitable due to the increase in the electrode surface to adhere.

On the other hand, the Si electrodes' electrical interface resistance and volumetric resistivity are improved by the MXene in the binder, as exhibited in Fig. 3-9 (b). The volume resistivity and interface resistance of the Si electrode containing the MC-HCS binder are 3.97×10^{-2} Ω cm and 4.93×10-5 Ω cm^2, respectively, which are the lowest among those containing the other biners, including conventional SBR binder. This illustrates that introducing conductive MXene to a water-based binder can improve the electrode conductivity and adhesion by the empty-core structure compared to the conventional core-shell SBR binder.

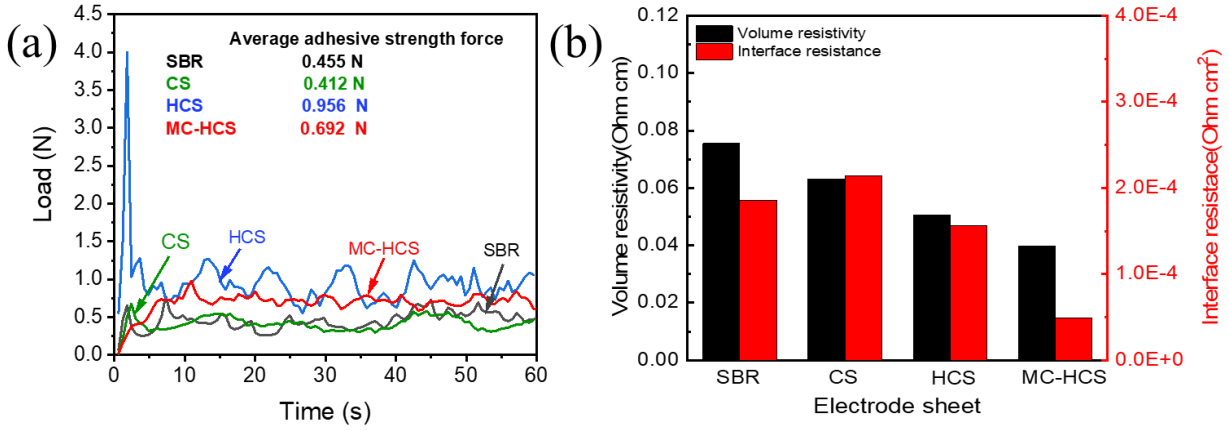

Figure. 4-9 (a) The adhesion strength and (b) The electrical resistance of the silicon electrodes composed of different binders.

4.2.3 Electrochemical characterization

The electrochemical performances of the Si anodes examine using CR2032-type coin-half cells at room temperature. As displayed in Fig. 4-10, all CV curves of the Si electrodes show similar electrochemical behaviors. Wide cathodic peaks in the first cycle are observed in the voltage range of 0.5–1.5 V, which attributes to electrolyte decomposition and the SEI layer formation [95–97]. However, the peaks disappear in the following cycles, explaining that the SEI layer on the surface of active materials has completed at the first cathodic sweep. The sharp anodic peaks around 0.58 V are associated to the de-lithiation of amorphous Li_xSi, and there also presents clear cathodic peaks around 0 V, corresponding to the lithiation of Si.

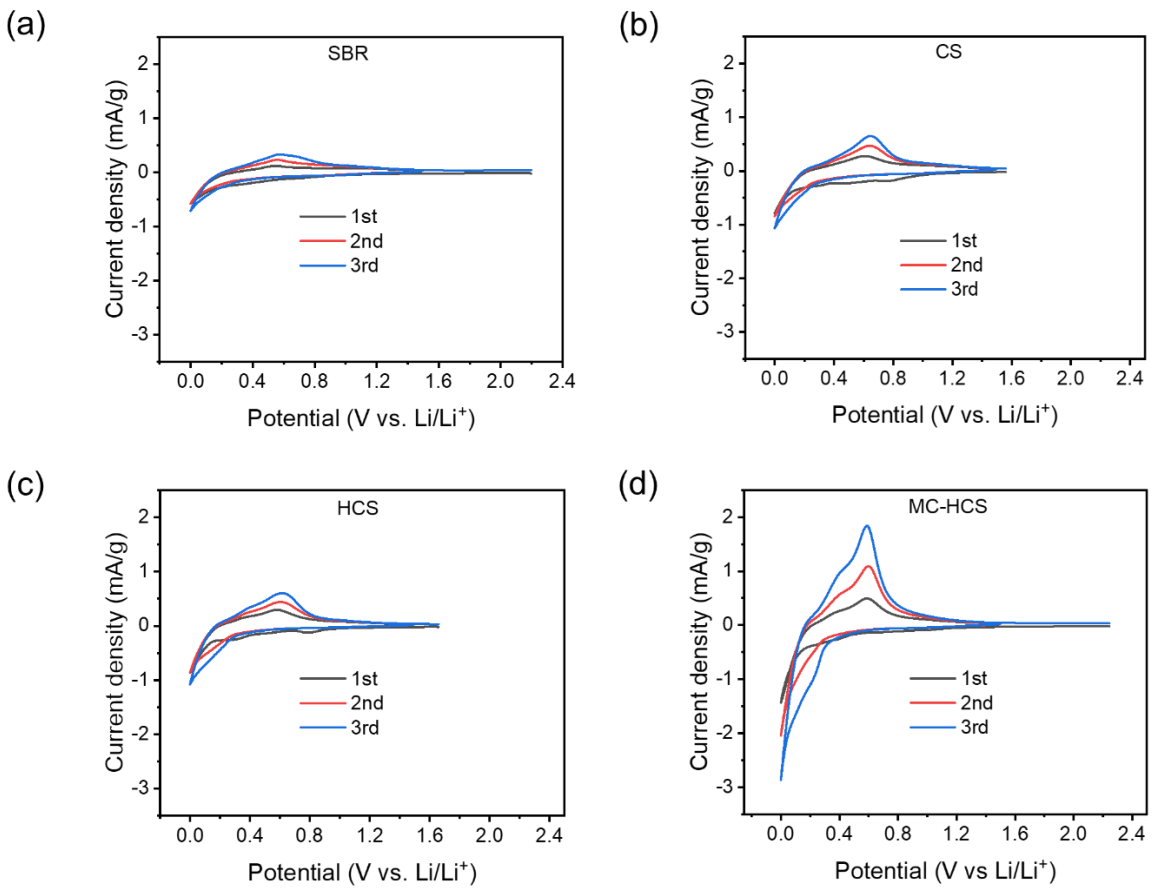

Figure. 4-10. The CV profiles of the silicon electrodes containing different binders. (a) SBR, (b) CS, (c) HCS and (d) MC-HCS electrodes.

To compare the electrochemical activity in the different binders of the Si electrodes, the third CV profiles of the silicon electrodes containing different binders are selected and redraw in Fig. 4-11 (a). The MC-HCS-containing Si electrode exhibits distinct redox peak intensities resulting from lithiation and de-lithiation of Si, whereas the other electrodes show sluggish CV profiles. In addition, the difference in the redox peak potentials is smaller than any other electrodes. Therefore,

introducing MCs facilitates redox reactivity due to its high electronic conductivity [98].

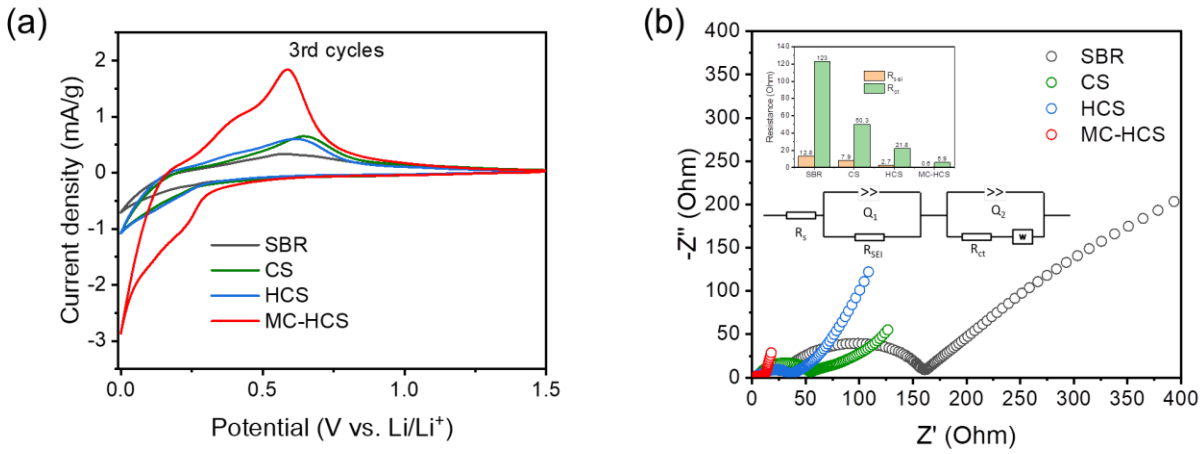

Fig. 4-11. Electrochemical performances of the Si electrodes composed of different binders: (a) CV profiles of the third cycles, (b) EIS spectra of the 100 cycled Si-based electrodes

The electrochemical impedance of the 100 cycled cells operates at 0.2 V with amplitude of 7 mV. The Nyquist plots shown in Fig. 4-11 (b) consist of three main regions: two compressed semicircles corresponding to the solid interfacial resistance (R_{sei}) in the high frequency range and the charge transfer resistance (R_{ct}) in the middle-frequency range, respectively, and a straight line in the low frequency range belongs to the diffusion of lithium ions [95]. As shown in the insert in Fig.4-11 (b), the R_{sei} of SBR-, CS, HCS and MC-HCS-containing Si electrodes are 12.8, 7.9, 2.7, and 0.6 Ω, respectively. Compared to the CS electrode, the HCS and MC-HCS

electrodes have much smaller R_{sei}, implying that MXenes in electrodes can keep integrated electrical network and prevent the formation of a thick SEI layer on the surface of silicon particles. A thick SEI layer is unstable and cannot tolerate volumetric expansion during lithiation and de-lithiation [99]. The electrode fabricated with an HCS binder shows a lower charge transfer resistance of 21.8 Ω compared to SBR 123 Ω and CS 50.3 Ω, attributed to the good ionic conductivity and high adhesive strength of HCS in Fig. 4-7 and 4-9 (a) [100,101]. Furthermore, the R_{ct} value of 5.9 Ω of the MC-HCS electrode becomes smaller than that of the HCS electrode. Such a low charge transfer resistance must be influenced by high ionic conductivity and low resistance in Fig.4-7 and 4-9 (b) [62,102,103]. In summary, the hollow core-shell structure is facile for ions to transport in the Si electrode, and the existence of MC is helpful to constructing electrical network of the Si electrodes.

Figures 4-12 (a) and (b) show the cycling performance and rate capability of Si-based electrodes with different binders. All electrodes were charged/discharged at 0.1C for the first two cycles and 0.5C for the subsequent 100 cycles. Stable coulombic efficiency is an essential parameter for long cycling performance. The electrodes with the MC-HCS binder display ascending coulombic efficiency (more than 95% since 3rd cycle and keep around 98% after 50 cycles), while others show low ascending coulombic efficiency (lower than 90% at 3rd cycle and lower than 95%

after the cycles). As a result, the MC-HCS electrode shows superior capacity retention of 1351 mAg^{-1} at 0.5C after 100 cycles. In contrast, the HCS electrode is 713 mAh g^{-1}, and the CS and SBR electrodes are only 203 mAh g^{-1} left. The electrodes without MC exhibit rapid capacity fading during 100 cycles, often detected when cracks in the high-capacity electrode led to electrical isolation. On the other hand, the MC-HCS electrode shows a more stable cycling capacity, indicating that the conductive MC in the binder maintains electrical networks even in the cracked electrode. Those phenomena were observed in the rate capability test shown in Fig. 4-12 (b). The MC-HCS electrode provides better rate capability than others. The capacity drop of the MC-HCS are much smaller than the others, even at a high current density of 5C, and the electrode maintains capacity retention of 1100 mAh g^{-1}. On the contrary, the capacities of HCS, CS, and SBR electrodes decrease rapidly as the current density increases. Also, at 5C, it dramatically drops to 750 mAh g^{-1} for HCS electrodes, and less than 250 mAh g^{-1} for CS and SBR electrodes. The Si electrode containing the MC-HCS binder recovers its potential very well when the current drops to 0.1C. It should be noticed that the contribution of MCs to the capacity is negligible because its amount is 0.167wt.% in electrode and the theoretical capacity of bare MCs is reltively small (320 mAh g^{-1}) [104].

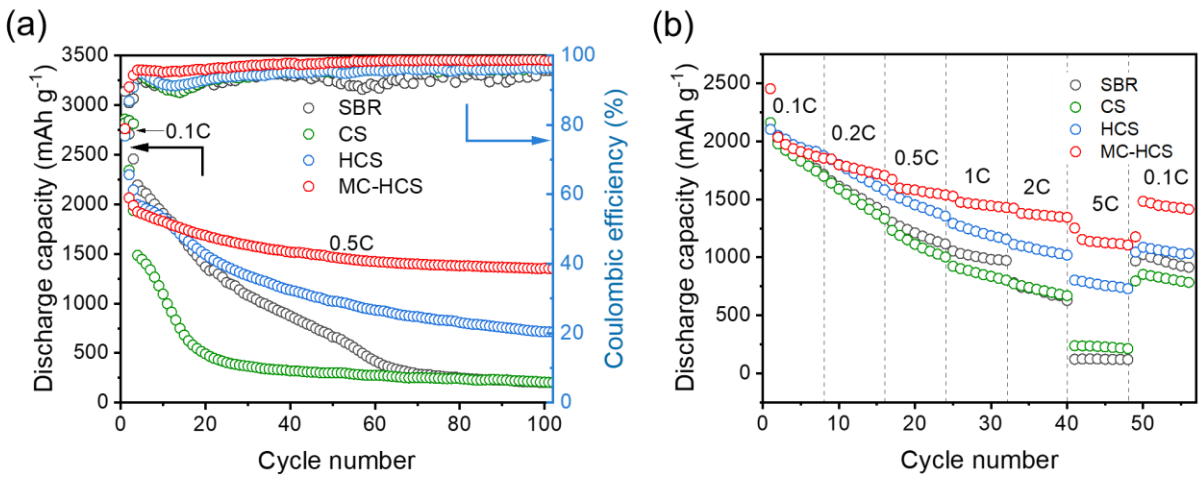

Figure. 4-12. Electrochemical performances of the Si electrodes composed of different binders (a) cycling performance, and (b) rate capability.

Different amounts of MCs were physically mixed with HCS binder during the slurry preparation process to further investigate the effects of in-situ polymerized binder on MCs. Regardless of the physically mixed MCs amount, the binder content, including MCs, maintains 10 wt% in electrodes. Thus, the HCS/MC-0.5%, 1%, and 2% samples contains HCS and MCs 9.5%:0.5%, 9%:1%, and 8%:2% in the electrodes, respectively. The electrochemical performances are exhibited in Fig.4-13 (a) and (b). As expected, the increase in the amount of physically mixed MCs decreases the impedance of the Si electrode, as shown in Fig. 4-13 (a). However, their R_{sei} and R_{ct} are much larger than those of the Si electrode fabricated by the in-site polymerized MC-HCS binder (Fig. 11 (b)). Moreover, the cycling performance

test results show much worse regardless of the amount of the physical mixed MCs compared to the MC-HCS-containing Si electrode, as shown in Fig. 4-13 (b). These indicate that physically mixed MC could not prevent the loss of reversible storage sites due to the electrical isolation [105]. As seen in Figure 4-14, MCs is not homogenously dispersed in the HCS binder solution and is rather sedimented. On the contrary, the in-situ polymerized MC-HCS binder is well dispersed and looks stable in the solution, as shown in Fig. 2-1. Above all, the homogeneous dispersion of MC-HCS binder could maintain the electrical network even during the charge/discharge process of Si accompanying huge volume change.

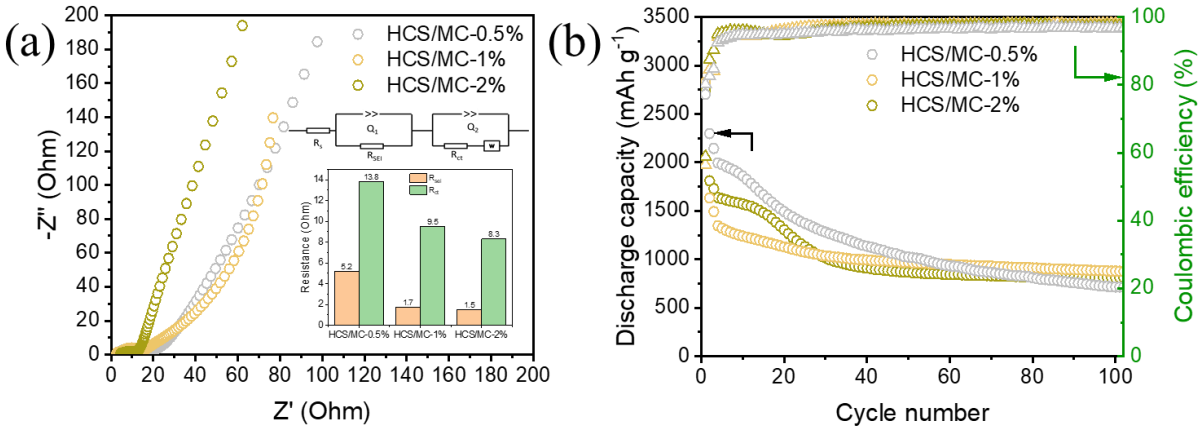

Figure 4-13 The EIS spectra and cycling performance of the Si electrodes fabricated with different amount of physically mixed MCs are shown in (a) and (b), respectively.

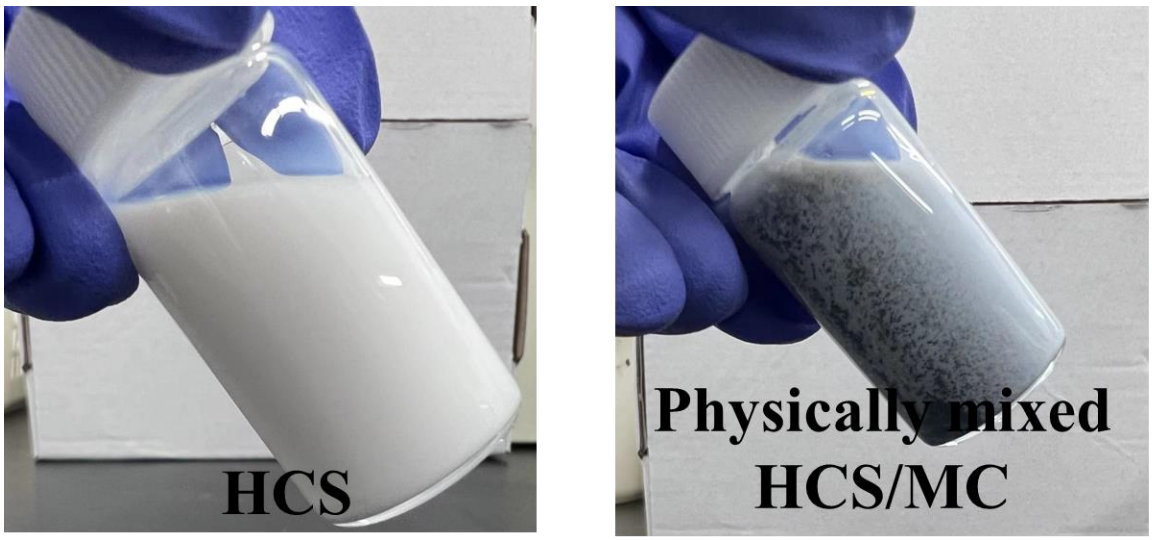

Figure 4-14. photographs of HCS binder (left) and physically mixed HCS/MC (right).

SEM images was taken to better investigate the morphological evolution during cycling. According to the top-viewed SEM images shown in Fig. 5(a-h), all electrodes with different binders exhibit unbroken and smooth surfaces before charge/discharge cycle. However, after 50 cycles, the electrodes with SBR, CS and HCS appear serious cracks. In contrast, the electrodes fabricated using MC-HCS binder maintains the structure integral and crack-free morphology. The volume expansion rate of electrodes was calculated from cross-sectional SEM analysis shown in Fig. 5(i-p). The thickness change of Si electrodes containing SBR, CS, HCS and MC-HCS are 13.51 μm, 15.30 μm, 10.27 μm, and 5.15 μm, respectively. Thus, the MC-HCS electrodes demonstrate the lowest volume expansion rate of 36%

compared to the electrodes of SBR (100%), CS (124%), and HCS (68%) electrodes. Such phenomena indicate that the MC-HCS binder could enable silicon surface stable by providing complete electrical network and alleviating thick SEI layer formation, together with avoiding silicon particle broken and structure collapse.

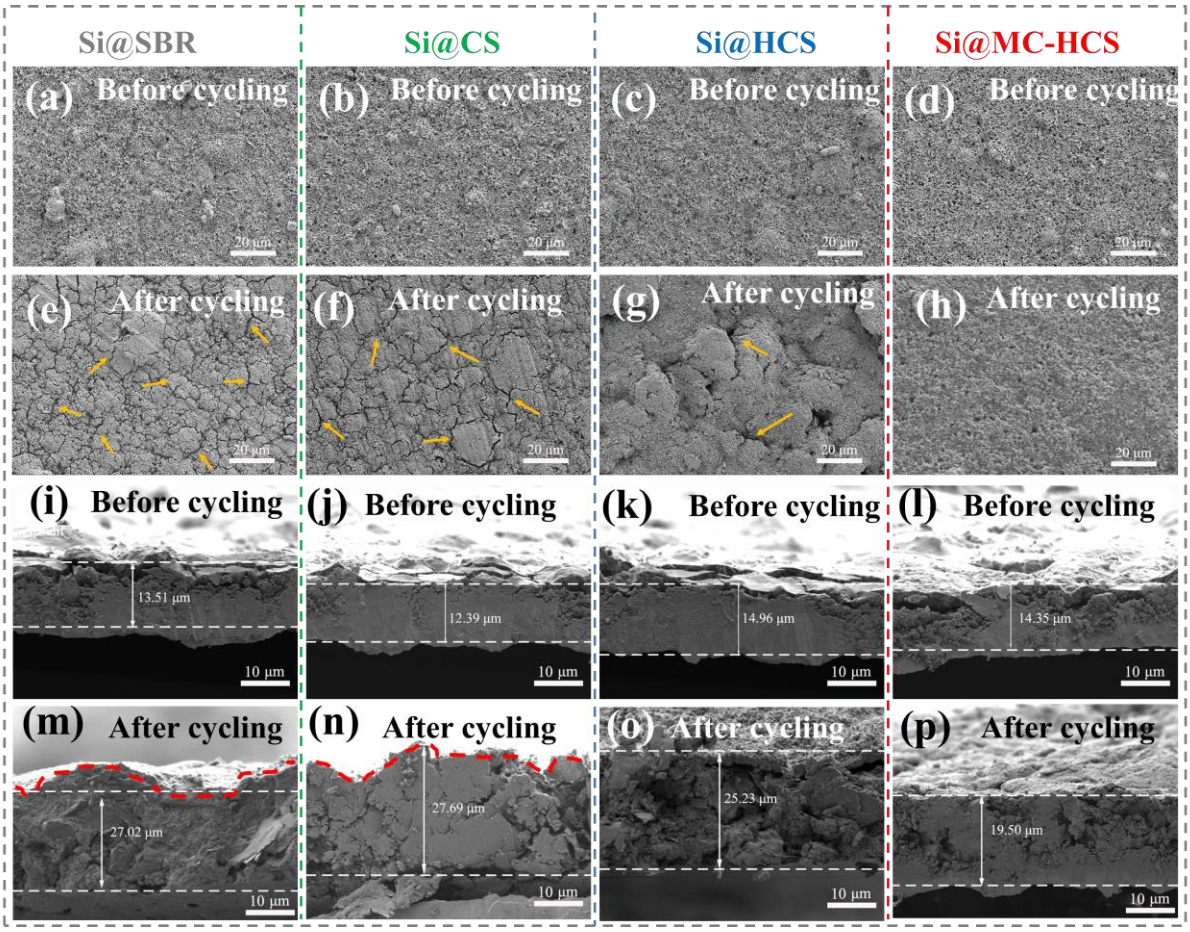

Figure. 4-15. The top-viewed SEM images of the Si electrodes with (a) SBR, (b) CS, (c) HCS and (d) MC-HCS before cycling, and (e) SBR, (f) CS, (g) HCS and (h) MC-HCS after 50 cycles. The cross-sectional images of the Si electrodes with (i) SBR, (j) CS, (k) HCS and (l) MC-HCS

before cycling, and (m) SBR, (n) CS, (o) HCS and (p) MC-HCS after 50 cycles.

4.3 Conclusion

We have successfully developed an MXene clay/water-based acrylate composite binder for silicon anode. The addition of MXene clay alleviates the electrical isolation of silicon electrodes after the huge volumetric change, and the hollow core-shell structure of the polymer could improve ionic conductivity. Moreover, the in-situ polymerized MC-HCS binder makes the MXene clay and acrylate binder connect strongly and homogeneously rather than providing a weak connection through physical blending. These ensure that MC-HCS binder is appropriate to electrolyte affinity and better ionic conductivity and guarantees excellent electrochemical performance in high-capacity silicon anode. The high-capacity retention, 1351 mAh g^{-1} after 100 cycles at 0.5C, of silicon electrodes containing MC-HCS binder is approximately 2 times greater than that containing HCS with no MCs, which is much larger than those containing CS with no MCs and no hollow core as well as the commercial SBR binder. The in-situ acrylate polymerization with MCs is much more favorable to the electrochemical performance of the binder when compared to the physical mixing of MCs with the acrylate binder. The novel strategy of combining conductive MXene and adhesive

water-dispersed acrylate binder by the in-situ emulsion polymerization provides a new way to design and synthesize eco-friendly water-based binder for high-capacity silicon anodes.

5 Tannic acid cross-linked zwitterionic copolymer binder

5.1 Introduction

Silicon with variety of advantages such as high theoretical capacity (~4200 mAh/g), low operation potential (< 0.5 V vs. Li/Li^+), and abundant resources has been widely studied as anode materials[106,107]. but its application is hindered by its huge volume expansion (~300%) during lithiation and de-lithiation[108,109]. Once the huge volume expansion fails to be accommodated, the delamination between anode components and current collector, pulverization of Si particles, thick SEI layer on Si surface could occur in silicon-based electrodes. The delamination influences electrons' delivery in electrodes and causes electrical isolation[110]. The pulverization generates dead silicon segments and result in dramatic capacity loss[111]. Thick SEI layer consumes more Li ions and leads to low Li^+ diffusion[112]. Those deteriorate the electrochemical performance of silicon-based electrodes.

To tackle aforementioned problems, the one way is to make efforts on the preparation of silicon-based electrode such as the design on silicon structure and the

combination use with graphite[113–115]. Although significant reports have demonstrated the improvement of silicon structure, it is difficult to realize due to its complicated procedure and high cost. Graphite with a reversible capacity of 372 mAh g^{-1} has been widely and commercially used as anode materials due to its high conductivity and excellent reversibility[116]. But in practical application, the huge volume change of silicon still influences the structural stability of silicon and graphite composite (Si/C) electrodes and further causes dramatic capacity fade during charging and discharge. The design of polymeric binder is another viable method. Polymeric binder could combine electrode components (e.g. active materials, conductive materials and etc.) and adhere electrode components to current collector. Therefore, the adhesion and structural design of binder could effectively alleviate the huge volume change and maintain structural integrity of silicon-based electrodes. According to our previous research[117], the traditional Poly (vinylidene fluoride) (PVDF) binder could not satisfy the demands in lithium-ion batteries (LIBs) nowadays because of its weak binding force with active materials surface and organic solubility in taxic solvent. Water-based polymeric binders such as poly acrylic acid (PAA), polysaccharides, carboxymethyl cellulose lithium (CMC-Li) and so on have been widely studied in LIBs[118–120]. However, those leaner polymeric binder lacks of deformation ability and easily result in the structure broken[121]. Branched and multi-dimensional polymeric binder could provide more contacts with

silicon surface and distribute stress force to side chains during volume expansion of silicon in lithiation process. What's more, multi-dimensional structure could integrate the functionalities of main chains and side chains. Therefore, it is possible for branched and multi-dimensional binders to offer multiple functionalities such as conductivity, desirable mechanical properties, good electrolyte affinity, etc. As reported, the branched polymeric binder could be archived by grafting side chains to main micromolecular chains, and multi-dimensional polymer could be obtained by crosslinking using small molecular crosslinker[122,123].

Tannic acid (TA) has lots of phenolic hydroxyl groups (Ph-OH). As well-known, Ph-OH groups could capture free radicals[124,125]. Therefore, in this study, it was used as crosslinker to connect with polyvinyl alcohol (PVA) and the copolymer of Sulfobetaine methacrylate (SBMA) and arylamide (AAm) (SBAAm) by active sites on polymer chains and hydrogen bonding. Where, PVA provides high mechanical strength and abundant hydroxy groups. The copolymer SBAAm with both SBMA and AAm segments exhibit the following functionalities: (1) good Li^+ diffusion efficiency due to the zwitterionic groups of SBMA, (2) high flexibility of AAm to distribute the stress of volume expansion and (3) strong adhesive strength because of hydrogen bonding with abundant amide groups ($-NH_2$). TA crosslinked PVA/SBAAm (abbreviated as TA-c-PVA/SBAAm) has a stable 3D framework with high flexibility and strong adhesive strength to alleviate the huge volume change and

maintain structure integral in silicon-based electrodes. Furthermore, TA-c-PVA/SBAAm are expected to improve Li^+ transport. the electrochemical performances of silicon-based anode could be improved simultaneously.

5.2 Results and discussion

5.2.1 Confirmation of synthesis

The synthesis of TA-c-PVA/SBAAm is schematically shown in figure 5-1. the hydroxyl groups (-OH) on PVA backbone were triggered by APS as initiator, where the APS was firstly decomposed to form anionic radicals which could attack -OH groups on PVA backbone and remove hydrogen of -OH to expose free radicals (-O·). At the same time, SBMA and AAm did copolymerization to form a copolymer of SBAAm with free radicals of -C·. Before those free radicals were inactivated, TA added and captured free radicals to construct a 3D framework of TA-c-PVA/SBAAm, in which TA functions as a bridge connect with rigid PVA and flexible SBAAm chains by covalent bonds of C-O-C. The stress from silicon particles' expansion could be distributed from chain to chain and accommodate volume change of silicon. What's more, the single direction ionic conductivity of SBMA facilitates the Li ions transportation by the coordination between Li^+ and SO_3^-.

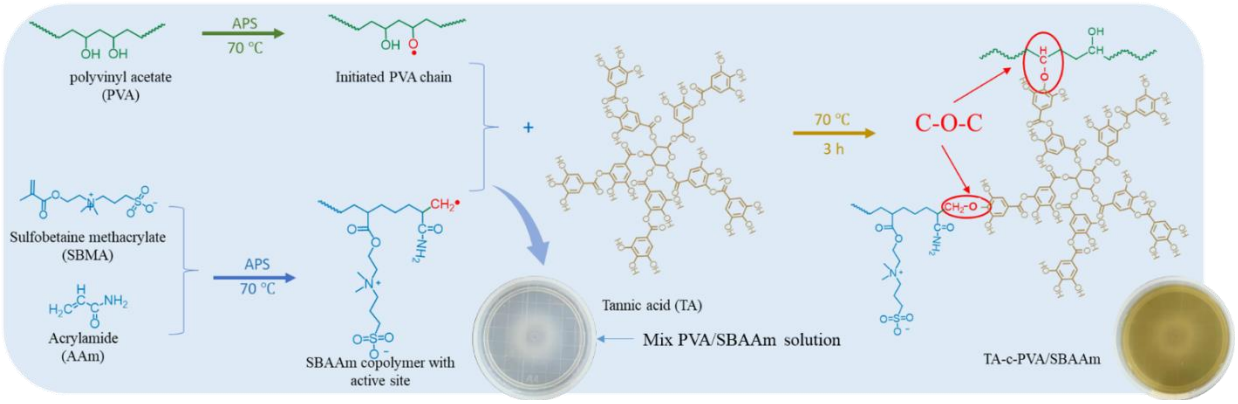

Figure 5-1 schematic for polymerization of crosslinked TA-c-PVA/SBAAm

FTIR spectra of PVA, the physical mixture of PVA and SBAAm (mix PVA/SBAAm) and TA-c-PVA/SBAAm are investigated in figure 5-2. Pure PVA has typical peaks at 3100-3250, and 1647 cm^{-1}, which are attributed to the stretching and bending vibration of -OH groups, respectively. The characteristic peaks of Ph-OH groups of TA could be observed at 1321 cm^{-1}, the aromatic double bones of phenol appear at 1446 and 1608 cm^{-1}. To confirm the successful crosslinking of TA to PVA and SBAAm, the physically mixed PVA and SBAAm also prepared as a comparison. Those vibration for SBAAm observes at 1041 and 1665, 1730 cm^{-1} corresponding to -S=O, -C-N+ and C=O groups, respectively. What's more, the absorption peak at 3200-3400 cm^{-1} assigned to the stretching of $-NH_2$. All characteristic vibrations for both pure PVA and physically mixed PVA/SBAAm could be observed in TA-c-PVA/SBAAm spectra. Typically, the new peak of C-O-C at 1197 cm^{-1} only exists in

TA-c-PVA/SBAAm spectra, which attribute to the crosslinking sites of TA to PVA and SBAAm. This explains that TA crosslink with PVA and SBAAm through covalent C-O-C bonds.

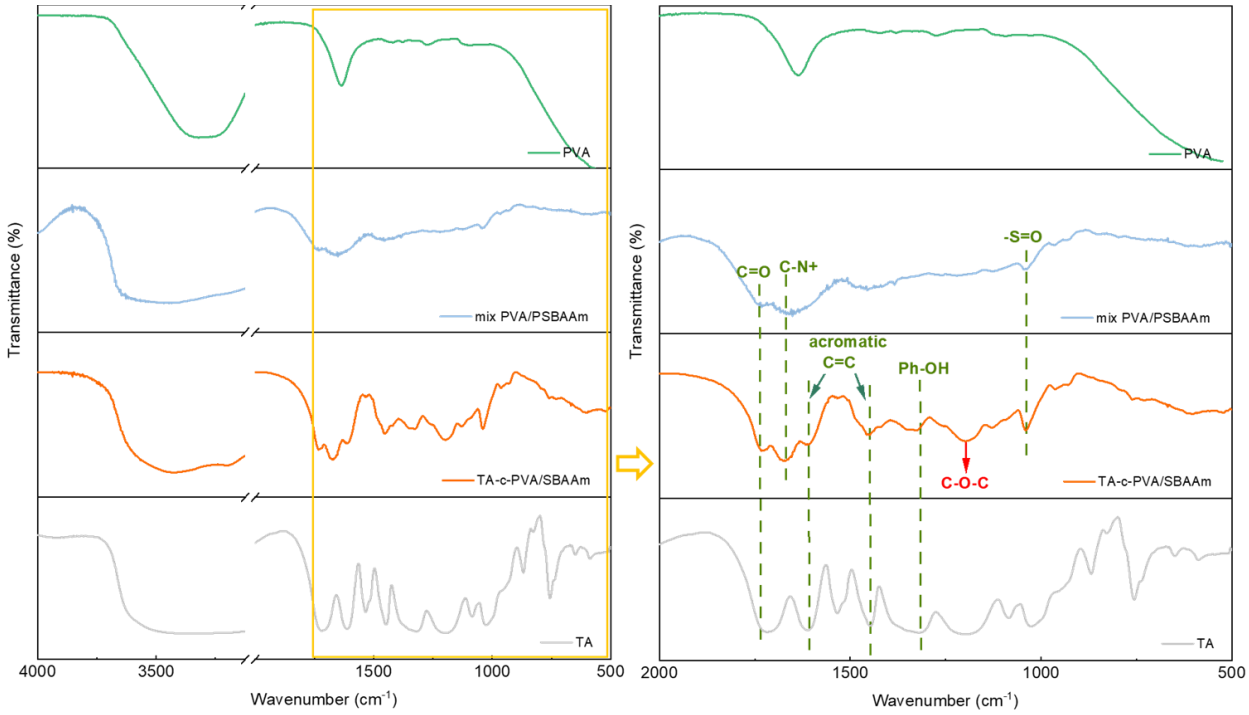

Figure 5-2 FTIR Spectro for PVA, TA, mix PVA/SBAAm and TA-c-PVA/SBAAm

5.2.2 Physical characterization

The viscosity of binder influences slurry preparation, electrode coating and thickness control. therefore, appropriate viscosity of synthetic binder is an important parameter. The results are shown in figure 3 (a). With the formation of 3D framework

of TA-c-PVA/SBAAm, it exhibits the highest viscosity of 6.7 Pa s comparing to physical mixed PVA/SBAAm (5.4 Pa s) and pure PVA (0.5 Pa s).

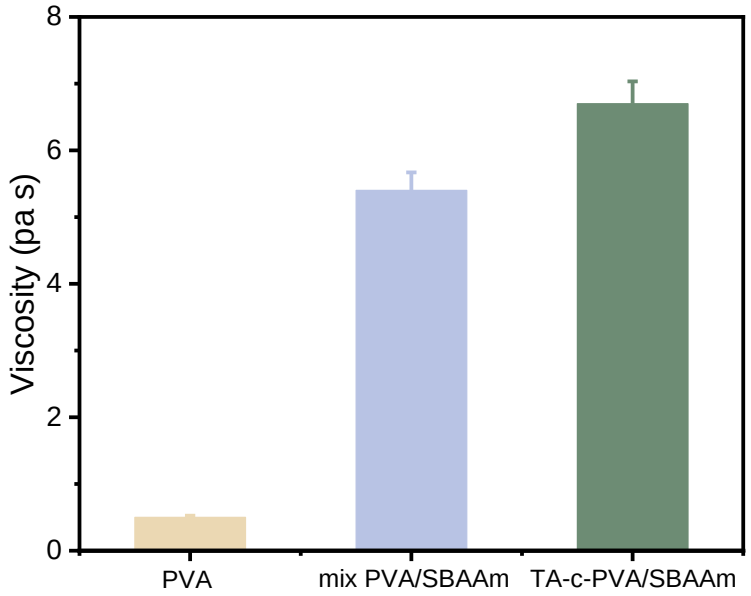

Figure 5-3 viscosity of PVA, mixed PVA/SBAAm and TA-c-PVA/SBAAm

Electrolyte uptake is related to the affinity between binder and electrolyte, and influences polymer binder's mechanical properties and Li ions transport in electrodes. It was calculated by immersing the binder films into organic electrolyte solution for 24 hours. According to figure 5-4, pure PVA reaches approximately 13.9%, whereas physically mixed with PVA/SBAAm shows lower electrolyte uptake of 6.4% due to the addition of SBAAm. SBAAm synthesized by random copolymerization of AAm and SBAA monomers. Both polymers are highly resistant

to organic electrolyte swelling. the crosslinked TA-c-PVA/SBAAm shows highest electrolyte uptake of 15.5% because of the crosslinked 3D network, which means the crosslinked TA-c-PVA/SBAAm polymer has better electrolyte swelling ability comparing to non-crosslinked polymers.

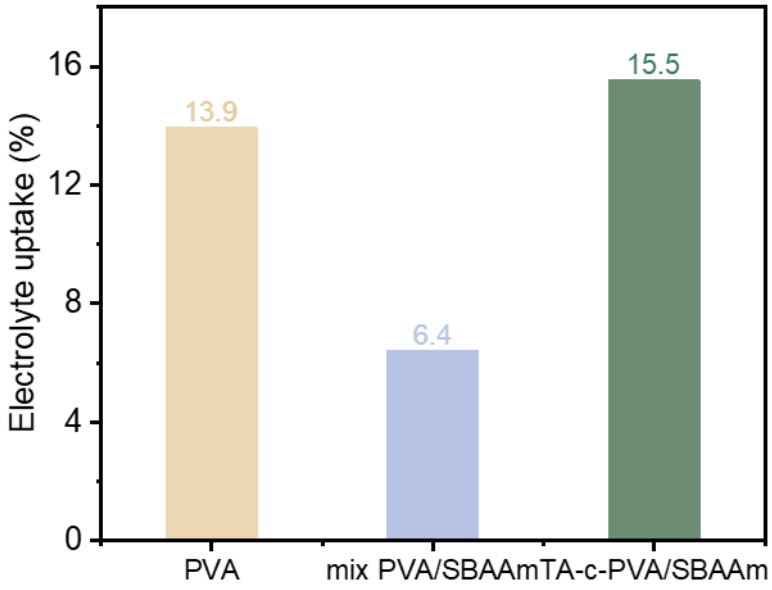

Figure 5-4 electrolyte uptake of PVA, mixed PVA/SBAAm and TA-c-PVA/SBAAm

The physical properties of Si/C electrodes were characterized through adhesive strength and electrical resistance to electrode sheets. the adhesive strength of Si/C electrodes with different binders was performed under 180° peeling tests using 2 cm wide electrodes strips with a peeling rate of 20 mm min^{-1}. As the result shows in figure 5-5, the average peeling strength for Si/C electrodes containing bare PVA and

mix PVA/SBAAm electrodes are 0.5 N and 0.75 N, respectively. the increase in adhesive strength attributes to abundant -NH_2 groups in SBAAm which provides more interaction points with silicon and graphite surface by hydrogen bonding. After the crosslinking of TA to PVA and SBAAm, the average adhesive strength of TA-c-PVA/SBAAm electrode increases to 1.5 N, which is 2 times higher than non-crosslinked PVA/SBAAm samples. This because the crosslinking makes the polymer chains interconnect stronger. 3D framework of TA-c-PVA/SBAAm could withstand the structural deformation when suffers external forces and strongly combine Si/C electrode components and current collector. So, TA-c-PVA/SBAAm binder with high adhesive strength is favorable to alleviate the huge volume change of silicon-based electrodes and stabilize Si/C electrode's structure over cycling.

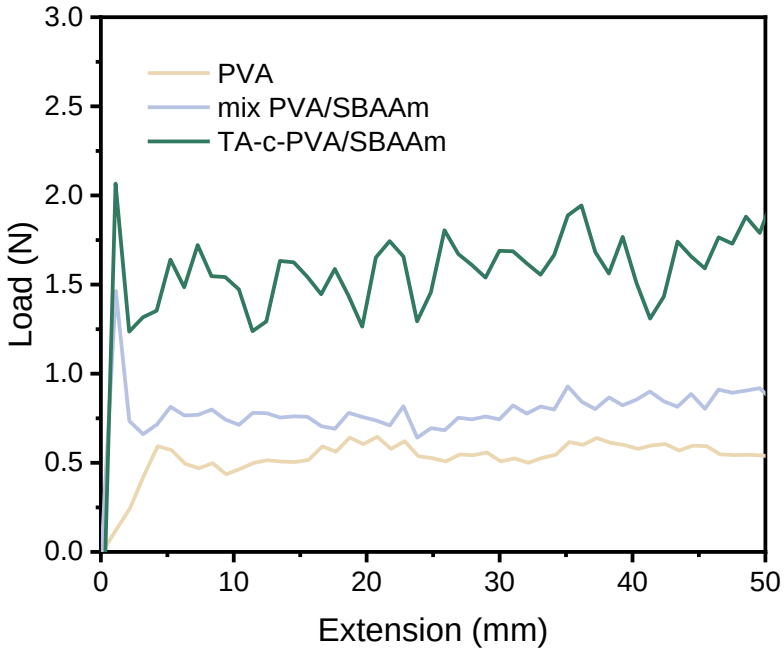

Figure 5-5 adhesion of electrodes with PVA, mixed PVA/SBAAm and TA-c-PVA/SBAAm binder

Electrical conductivity of Si/C electrodes predetermine the electrochemical performance. Therefore, the volume resistivity and interface resistance are investigated by 46 multi-probe measurement. The volume resistance reflects the electron delivery ability among electrode materials. The interface resistance is between current collectors and electrode component. As figure 5-6 shows, the Si/C electrodes with pure PVA binder show the highest volume resistivity of 8.31×10^{-2} Ohm cm and interface resistance of 7.4×10^{-3} Ohm cm^2. And both resistance and resistivity decrease for Si/C electrodes with physical mixed PVA/SBAAm binder.

the Si/C electrodes containing TA-c-PVA/SBAAm has the lowest volume resistivity of 4.37 × 10^{-3} Ohm cm and interface resistance of 7.67 × 10^{-5} Ohm cm^2. the results are consistent with the results of adhesive strength. This illustrates that the adhesive strength is stronger, the electrodes materials combine tighter, and the resistivity and resistance are smaller. the covalently crosslinked 3D framework of TA-c-PVA/SBAAm binder with high adhesive strength is better to construct the stability of electrical network in Si/C electrodes.

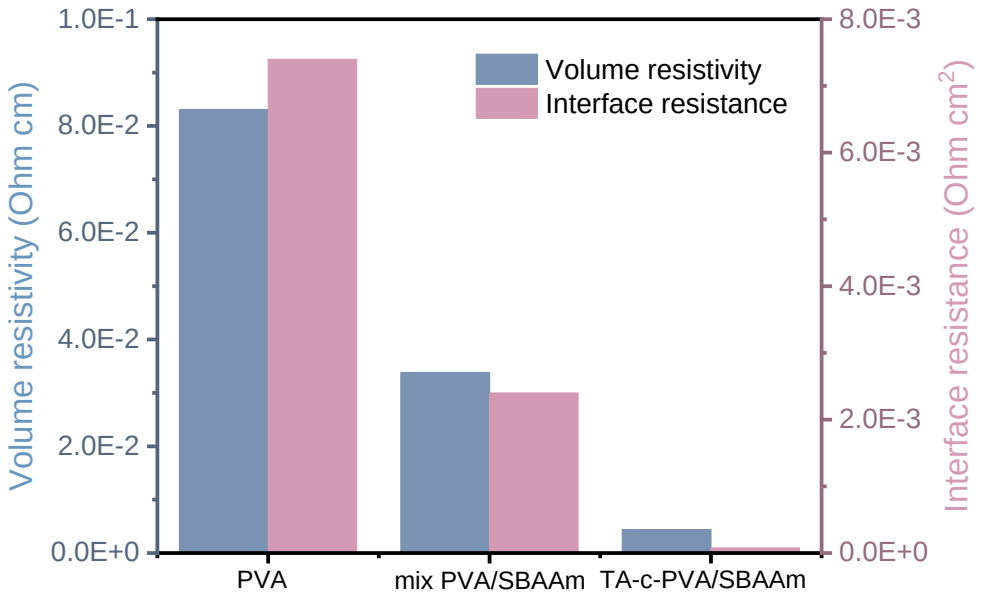

Figure 5-6 electrical resistance of electrodes with PVA, mixed PVA/SBAAm and TA-c-PVA/SBAAm binder

5.2.3 Electrochemical characterization

(d) electrical resistance of Si/C electrodes containing different binders.

To better understand the effect of SBAAm segment to TA-c-PVA/SBAAm binder in Si/C electrodes, ionic conductivity was explored by kinetics analysis. According to Randles–Sevcik equation (shown in equation 1), the diffusion coefficient (D_{Li^+}) could be calculated by the leaner slope of the redox peak current (I_p) and the square root of scanning rates at different scan rate ($V^{0.5}$). Figure 4 (a) and (b) show CV curves of PVA and TA-c-PVA/SBAAm electrodes at different scan rate from 0.05-0.5 mV s^{-1}, respectively. The leaner relationship of I_p-$V^{0.5}$ plots exhibits in figure 4 (c). the D_{Li^+} results display in figure 4 (d). the Si/C electrodes with TA-c-PVA/SBAAm binder show higher D_{Li^+} (5.4×10^{-4} cm^2 s^{-1} for anodic and 5.7 10^{-4} cm^2 s^{-1} for cathodic) than PVA electrodes (2.8×10^{-4} cm^2 s^{-1} for anodic and 3.8×10^{-4} cm^2 s^{-1} for cathodic). This demonstrates that the polymer chains of zwitterionic SBAAm in TA-c-PVA/SBAAm binder could improve lithium ions insertion/desertion in Si/C electrodes and further enhance overall cell's performance.

$$I_p = \left(2.69 \times 10^5\right) n^{1.5} A D_{Li^+}^{0.5} v^{0.5} C_{Li^+} \qquad \text{equation 1}$$

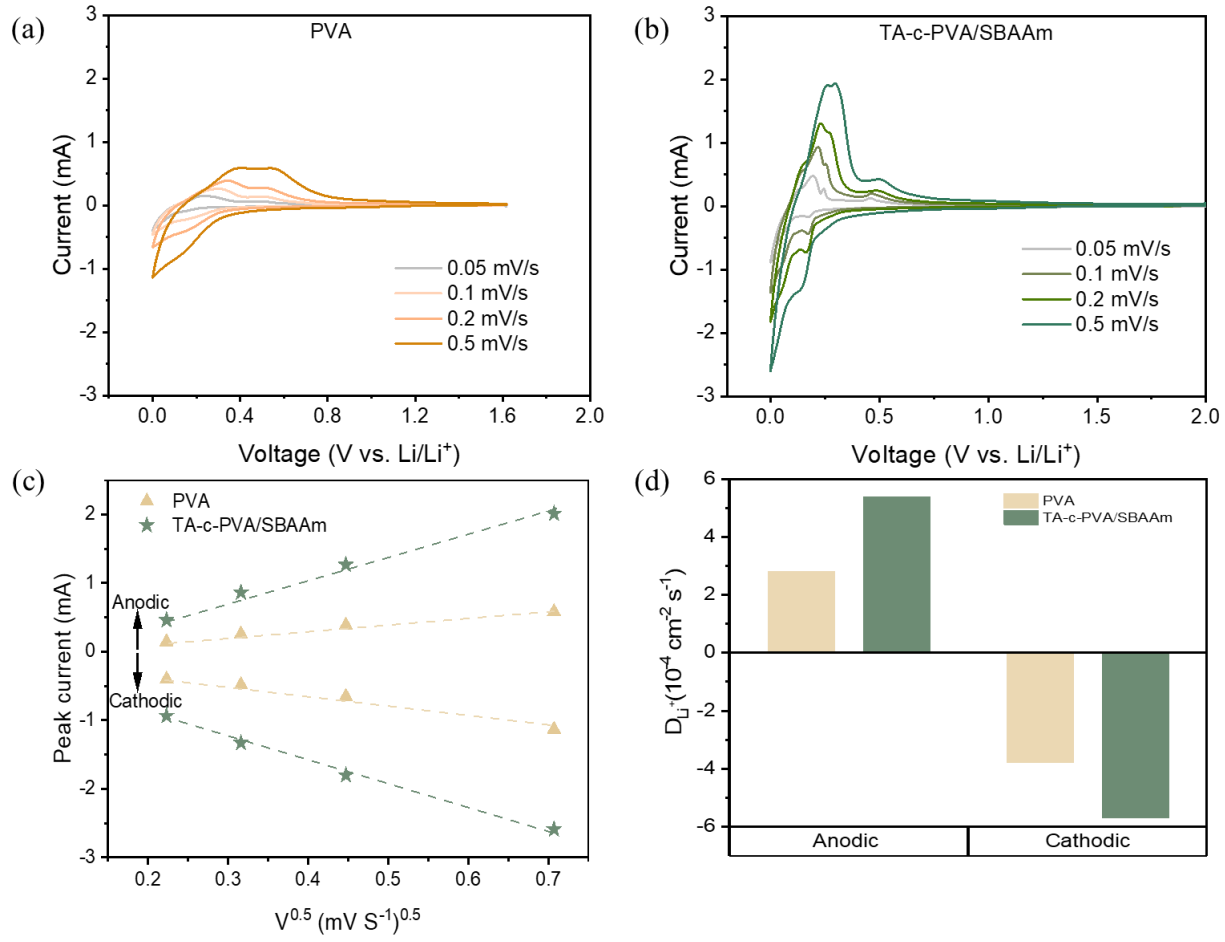

Figure 5-7 Li-ion diffusion coefficients of Si/C electrodes. a) CV curves of PVA electrodes (b) CV curves of TA-c-PVA/SBAAm electrodes at different potential scanning rates from 0.05 to 0.5 mV s^{-1}. (c) The relationship of peak current (I_p) versus square root of the potential scaning rates ($v^{0.5}$). (d) Comparison of the calculated D_{Li}^{+}.

The electrochemical performances of Si/C with different binders were further exanimated in CR2032 type coin cells. CV was firstly conducted under a scan rate of 0.5 mV/s from 0-1.5 V for three cycles. Figure 5-8 (a)-(c) show CV curves of the electrodes with PVA, mix PVA/SBAAm and TA-c-PVA/SBAAm binders,

respectively. All CV curves of Si/C electrodes with different binders show a pair of redox peaks, where the anodic peaks represent de-lithiation of amorphous Li_xSi. The peaks appear in cathodic scanning are associated to lithiation of Si. And for each first cycles, there are wide-range cathodic peaks in the voltage range of 0.25-1.25 V, due to the electrolyte decomposition and the SEI layer formation. What's more, we could observe that in the following cycles, it disappears and a sharp cathodic peak could be observed close to 0 V for all electrodes with different binders. However, the anodic peaks for different electrodes shows differences. For comparation, the third cycles are selected and shown in figure 5-8 (d). the oxidation of TA-c-PVA/SBAAm electrodes occurs earlier than the electrodes with other binders, which means the electrodes has smaller potential differences between redox peaks. this explains that the crosslinked TA-c-PVA/SBAAm binder is favorable to decrease the polarization resistance attributing to its high adhesive strength and low resistance in Si/C electrodes. Furthermore, the pure PVA electrodes show sluggish CV curves. In contrast, TA-c-PVA/SBAAm electrodes exhibit higher redox currents, which could be associated to the fast Li^+ diffusion by zwitterionic SBAAm polymer chain in TA-c-PVA/SBAAm.

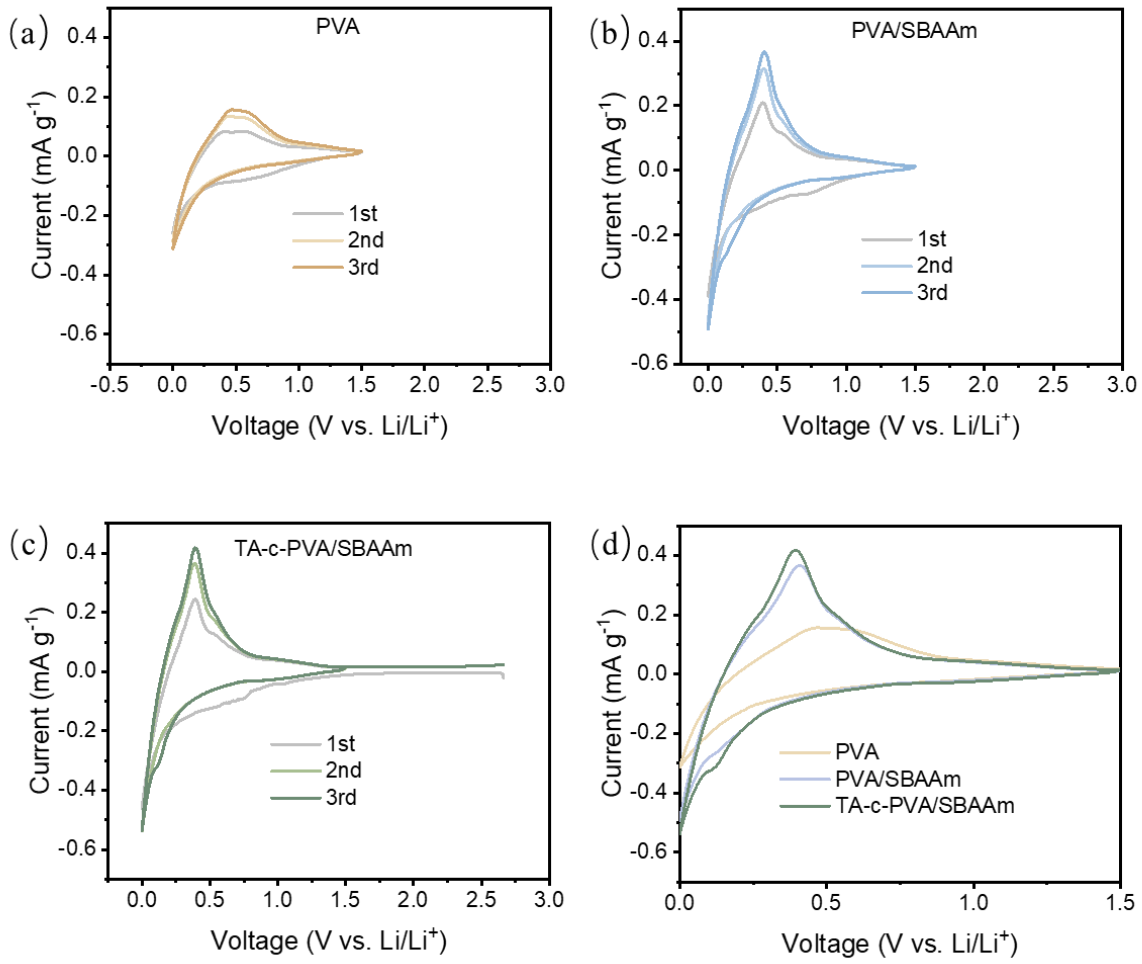

Figure 5-8 the CV curves of Si/C electrodes with different binders (a) pure PVA, (b) PVA/SBAAm, (c) TA-c-PVA/SBAAm, and (d)selected 3rd cycles

As shown in figure 5-9 (a), the electrodes with PVA, mix PVA/SBAAm and TA-c- PVA/SBAAm binder display initial coulombic efficiency (ICE) of 77.2%, 84.7% and 86%, respectively. Such high ICE of TA-c-PVA/SBAAm electrodes is beneficial for the improved ionic conductivity that effectively reduces the

consumption of Li ions in first cycle and enhances the reversibility of Li ions. The whole coulombic efficiency for the Si/C electrodes containing TA-c- PVA/SBAAm binder in 200 cycles is more stable and higher than others. This because the abundant function groups (-OH, -NH_2, etc.) in TA-c-PVA/SBAAm binder provide strong adhesive strength with silicon surface, and the crosslinked 3D network of TA-c-PVA/SBAAm binder could maintain electrode's structure stable that avoids electrical isolation of Si/C electrodes caused by the huge volume change of Si.

Figure 5-9 (b) shows the long-term cycling performance of Si/C electrodes with different binders at 0.1C for first 2 cycles and 0.5C (1C= 1250 mAh g^{-1}) for the following 200 cycles. the pure PVA containing Si/C electrodes shows the lowest capacity retention of around 200 mAh g^{-1} and sever capacity loss even in early cycles. When PVA physically mixed with SBAAm, the reversible capacity increase to 400 mAh g^{-1} after 200 cycles. This is because the polymer chain of SBAAm in binders facilitate lithium ions diffusion, and enhance cell cyclability. in particular, the crosslinked TA-c-PVA/SBAAm has highest capacity retention of approximately 700 mAh g^{-1} and could stably operate for 200 cycles comparing to others. Furthermore, we investigated the rate capability of Si/C electrodes with different binder under varied current density from 0.1C to 5C and back to 0.1C (1C= 1250 mAh g^{-1}). Figure 5-9 (c) illustrates that TA-c-PVA/SBAAm electrodes exhibit excellent rate capability, less capacity loss as current density increase, and could withstand high current

density up to 5C (with capacity retention of 687 mAh g^{-1}) while compare with non-crosslinked mix PVA/SBAAm electrodes (with capacity retention of 366 mAh g^{-1}). This describes that the binders with 3D network and covalent crosslinking dot could accommodate significant volume change of Si/C electrodes and promise integral electrical network.

Besides, the influence of different TA content in TA-c-PVA/SBAAm also is studied. The different crosslinking degree in binder causes different influences in electrodes. As the figure 5-9 (d) shows, all electrodes containing crosslinked TA-c-PVA/SBAAm binder has higher and more stable cycling performance comparing with non-crosslinked mix PVA/SBAAm which has been explained previously. When the amount of TA in TA-c-PVA/SBAAm binder increase from 1 wt% to 2 wt%, the capacity retention increases from 614 mAh g^{-1} to 770 mAh g^{-1}. However, the capacity retention and cycling performance are not as good as the increase of TA amount. when the content of TA increase to 4 wt%, the capacity loss faster, and the capacity retention decline more comparing to 2 wt%. this might because as the addition of more TA in TA-c-PVA/SBAAm, the crosslinking degree increase, the binder becomes more brittle. this result confirms that 2 wt% of TA in TA-c-PVA/SBAAm binder is considered as the best proportion of binder while apply to Si/C electrodes.

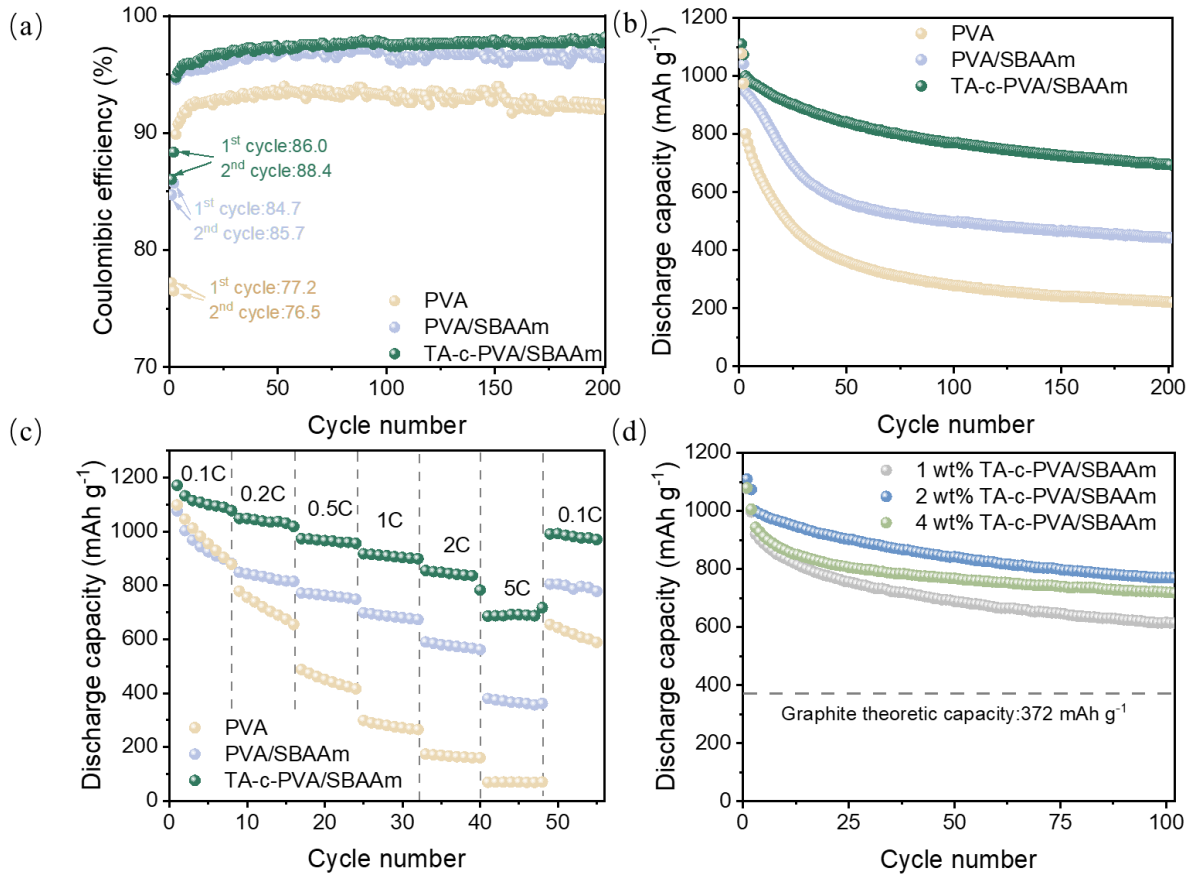

Figure 5-9 electrochemical performance of Si/C electrodes with different binders (a)coulumbic efficiency, (b) cycling performance, (c) rate capability, and (d)cycling performance of TA-c-PVA/SBAAm with different proportion TA

The interfacial stability of Si/C electrodes before and after cycling were investigated by top-view SEM images. all electrodes with different binders show integral surfaces before cycling in figure 5-10 (a-c). However, after 200 cycles, pure PVA electrodes shows severe structure collapse. And huge crakes could observe in mix PVA/SBAAm electrodes. In contrast, the electrodes with TA-c-PVA/SBAAm exhibit negligible cracks on the surface. Those results explain that the crosslinked 3D network binder provides effectively efforts on alleviating the volume changes, and ensures electrodes integral.

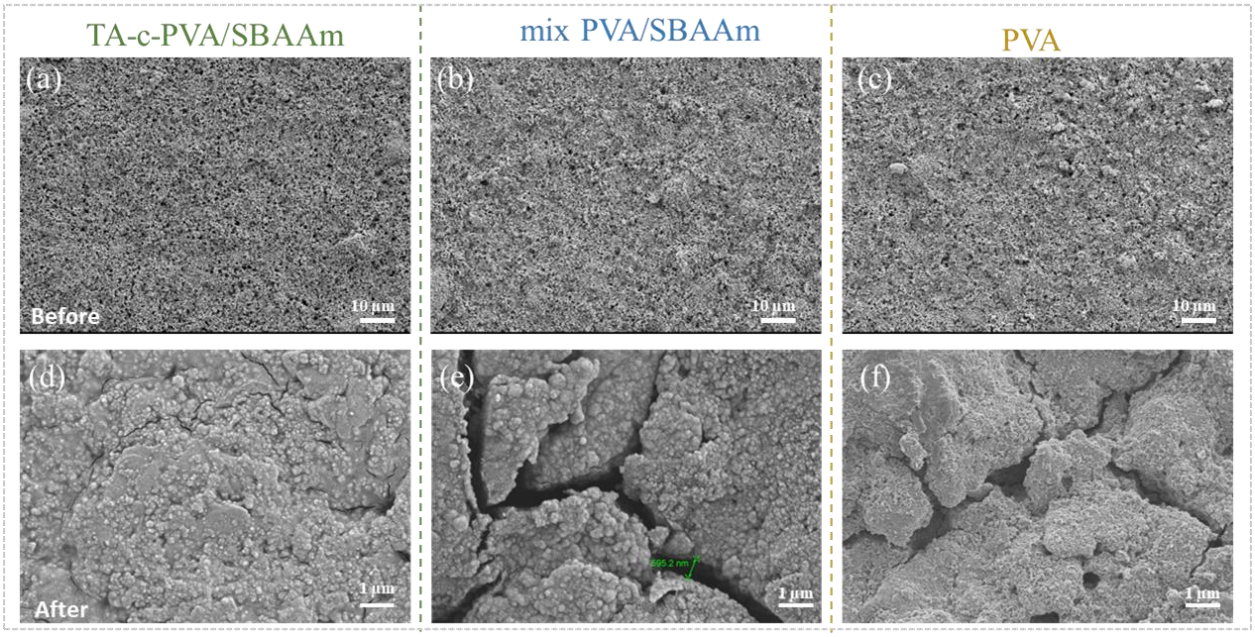

Figure 5-10 Top-view SEM images of Si/C electrodes with different binders

5.3 Conclusion

In summary, it has been confirmed that TA could be used as a crosslinker to construct a 3D framework by free radicals capturing. The crosslinked TA-c-PVA/SBAAm binder with 3D network improved the adhesive strength (2 times higher than non-crosslinked PVA/SBAAm) of Si/C electrodes which effectively alleviates the expansion of Si particles and attributes to less structural cracks and collapse. The introduction of zwitterionic SBAAm copolymer in TA-c-PVA/SBAAm binder facilitated Li^+ diffusion. The Si/C electrodes with TA-c-PVA/SBAAm binder illustrated high ICE (86%), stable cycling performance for 200 cycles at 0.5C, and excellent rate capability of 687 mAh g^{-1} at 5C. The new design strategy of 3D network binder provides a novel conception on polymer's multi-dimensional construction and emphasizes the synergy of all crosslinked polymer chains in Si/C electrodes.

6 Reference

[1] M.S. Whittingham, Electrical Energy Storage and Intercalation Chemistry, Science 192 (1976) 1126–1127. https://doi.org/10.1126/science.192.4244.1126.

[2] K. Mizushima, P.C. Jones, P.J. Wiseman, J.B. Goodenough, LixCoO2 (0<x<-1): A new cathode material for batteries of high energy density, Materials Research Bulletin 15 (1980) 783–789. https://doi.org/10.1016/0025-5408(80)90012-4.

[3] A. Yoshino, The Birth of the Lithium-Ion Battery, Angewandte Chemie International Edition 51 (2012) 5798–5800. https://doi.org/10.1002/anie.201105006.

[4] J. He, H. Zhong, J. Wang, L. Zhang, Investigation on xanthan gum as novel water soluble binder for LiFePO 4 cathode in lithium-ion batteries, Journal of Alloys and Compounds 714 (2017) 409–418. https://doi.org/10.1016/j.jallcom.2017.04.238.

[5] A. Barré, B. Deguilhem, S. Grolleau, M. Gérard, F. Suard, D. Riu, A review on lithium-ion battery ageing mechanisms and estimations for automotive applications, Journal of Power Sources 241 (2013) 680–689. https://doi.org/10.1016/j.jpowsour.2013.05.040.

[6] G. Zubi, R. Dufo-López, M. Carvalho, G. Pasaoglu, The lithium-ion battery: State of the art and future perspectives, Renewable and Sustainable Energy Reviews 89 (2018) 292–308. https://doi.org/10.1016/j.rser.2018.03.002.

[7] Y. Yang, E.G. Okonkwo, G. Huang, S. Xu, W. Sun, Y. He, On the sustainability of lithium ion battery industry – a review and perspective, Energy Storage Materials (2020). https://doi.org/10.1016/j.ensm.2020.12.019.

[8] A. Kraytsberg, Y. Ein-Eli, Conveying Advanced Li-ion Battery Materials into Practice The Impact of Electrode Slurry Preparation Skills, Advanced Energy Materials 6 (2016) 1600655. https://doi.org/10.1002/aenm.201600655.

[9] K. Wang, J. Wan, Y. Xiang, J. Zhu, Q. Leng, M. Wang, L. Xu, Y. Yang, Recent advances and historical developments of high voltage lithium cobalt oxide materials for rechargeable Li-ion batteries, Journal of Power Sources 460 (2020) 228062. https://doi.org/10.1016/j.jpowsour.2020.228062.

[10] J. Wan, J. Zhu, Y. Xiang, G. Zhong, X. Liu, Y. Li, K.H.L. Zhang, C. Hong, J. Zheng, K. Wang, Y. Yang, Revealing the correlation between structure evolution and electrochemical performance of high-voltage lithium cobalt oxide, Journal of Energy Chemistry 54 (2021) 786–794. https://doi.org/10.1016/j.jechem.2020.06.027.

[11] T. Matsuda, K. Ando, M. Myojin, M. Matsumoto, T. Sanada, N. Takao, H. Imai, D. Imamura, Investigation of the influence of temperature on the degradation mechanism of commercial nickel manganese cobalt oxide-type lithium-ion cells during long-term cycle tests, Journal of Energy Storage 21 (2019) 665–671. https://doi.org/10.1016/j.est.2019.01.009.
[12] J. Schmitt, A. Maheshwari, M. Heck, S. Lux, M. Vetter, Impedance change and capacity fade of lithium nickel manganese cobalt oxide-based batteries during calendar aging, Journal of Power Sources 353 (2017) 183–194. https://doi.org/10.1016/j.jpowsour.2017.03.090.
[13] H. Kim, K. Lee, S. Kim, Y. Kim, Fluorination of free lithium residues on the surface of lithium nickel cobalt aluminum oxide cathode materials for lithium ion batteries, Materials & Design 100 (2016) 175–179. https://doi.org/10.1016/j.matdes.2016.03.121.
[14] D. Wong, B. Shrestha, D.A. Wetz, J.M. Heinzel, Impact of high rate discharge on the aging of lithium nickel cobalt aluminum oxide batteries, Journal of Power Sources 280 (2015) 363–372. https://doi.org/10.1016/j.jpowsour.2015.01.110.
[15] A. Chagnes, B. Pospiech, A brief review on hydrometallurgical technologies for recycling spent lithium-ion batteries, Journal of Chemical Technology & Biotechnology 88 (2013) 1191–1199. https://doi.org/10.1002/jctb.4053.
[16] A. Manthiram, A reflection on lithium-ion battery cathode chemistry, Nature Communications 11 (2020) 1550. https://doi.org/10.1038/s41467-020-15355-0.
[17] H.C. Shin, W.I. Cho, H. Jang, Electrochemical properties of the carbon-coated LiFePO4 as a cathode material for lithium-ion secondary batteries, Journal of Power Sources 159 (2006) 1383–1388. https://doi.org/10.1016/j.jpowsour.2005.12.043.
[18] Y. Wu, Z. Wen, H. Feng, J. Li, Sucrose-Assisted Loading of LiFePO4 Nanoparticles on Graphene for High-Performance Lithium-Ion Battery Cathodes, Chemistry – A European Journal 19 (2013) 5631–5636. https://doi.org/10.1002/chem.201203535.
[19] X. Chen, Y. Li, J. Wang, Enhanced Electrochemical Performance of LiFePO4 Originating from the Synergistic Effect of ZnO and C Co-Modification, Nanomaterials 11 (2021) 12. https://doi.org/10.3390/nano11010012.
[20] Q. Jing, J. Zhang, Y. Liu, W. Zhang, Y. Chen, C. Wang, Direct Regeneration of Spent LiFePO4 Cathode Material by a Green and Efficient One-Step Hydrothermal Method, ACS Sustainable Chem. Eng. 8 (2020) 17622–17628. https://doi.org/10.1021/acssuschemeng.0c07166.
[21] P. Chand, S. Kumar, V. Singh, N.P. Singh, Investigation of the structural and electrical behavior of LiFePO4 as cathode material for energy storage

application, Materials Today: Proceedings 32 (2020) 483–486. https://doi.org/10.1016/j.matpr.2020.02.624.
[22] C. de la Torre-Gamarra, M.E. Sotomayor, J.-Y. Sanchez, B. Levenfeld, A. Várez, B. Laïk, J.-P. Pereira-Ramos, High mass loading additive-free LiFePO4 cathodes with 500 μm thickness for high areal capacity Li-ion batteries, Journal of Power Sources 458 (2020) 228033. https://doi.org/10.1016/j.jpowsour.2020.228033.
[23] H. Khalifa, S.A. El-Safty, A. Reda, A. Elmarakbi, H. Metawa, M.A. Shenashen, Multifaceted geometric 3D mesopolytope cathodes and its directional transport gates for superscalable LIB models, Applied Materials Today 19 (2020) 100590. https://doi.org/10.1016/j.apmt.2020.100590.
[24] Y.J. Nam, S.-J. Cho, D.Y. Oh, J.-M. Lim, S.Y. Kim, J.H. Song, Y.-G. Lee, S.-Y. Lee, Y.S. Jung, Bendable and Thin Sulfide Solid Electrolyte Film: A New Electrolyte Opportunity for Free-Standing and Stackable High-Energy All-Solid-State Lithium-Ion Batteries, Nano Lett. 15 (2015) 3317–3323. https://doi.org/10.1021/acs.nanolett.5b00538.
[25] B. Hu, I.A. Shkrob, S. Zhang, L. Zhang, J. Zhang, Y. Li, C. Liao, Z. Zhang, W. Lu, L. Zhang, The existence of optimal molecular weight for poly(acrylic acid) binders in silicon/graphite composite anode for lithium-ion batteries, Journal of Power Sources 378 (2018) 671–676. https://doi.org/10.1016/j.jpowsour.2017.12.068.
[26] Y. Qi, M.H.T. Nguyen, E.-S. Oh, Enhancement of the lithium titanium oxide anode performance by the copolymerization of conductive polypyrrole with poly(acrylonitrile/butyl acrylate) binder, J Appl Electrochem 50 (2020) 431–438. https://doi.org/10.1007/s10800-020-01401-8.
[27] W.-F. Ren, J.-B. Le, J.-T. Li, Y.-Y. Hu, S.-Y. Pan, L. Deng, Y. Zhou, L. Huang, S.-G. Sun, Improving the Electrochemical Property of Silicon Anodes through Hydrogen-Bonding Cross-Linked Thiourea-Based Polymeric Binders, ACS Appl. Mater. Interfaces (2020). https://doi.org/10.1021/acsami.0c18743.
[28] E. Markevich, G. Salitra, D. Aurbach, Influence of the PVdF binder on the stability of LiCoO2 electrodes, Electrochemistry Communications 7 (2005) 1298–1304. https://doi.org/10.1016/j.elecom.2005.09.010.
[29] B. Han, M.J. Piernas-Muñoz, F. Dogan, J. Kubal, S.E. Trask, I.D. Bloom, J.T. Vaughey, B. Key, Probing the Reaction between PVDF and LiPAA vs Li7Si3: Investigation of Binder Stability for Si Anodes, J. Electrochem. Soc. 166 (2019) A2396–A2402. https://doi.org/10.1149/2.0241912jes.
[30] M. Wang, Z. Xu, Y. Hou, P. Li, H. Sun, Q.J. Niu, Fabrication of a superhydrophilic PVDF membrane with excellent chemical and mechanical stability for highly efficient emulsion separation, Separation and Purification Technology 251 (2020) 117408. https://doi.org/10.1016/j.seppur.2020.117408.

[31] D.L. Wood, J.D. Quass, J. Li, S. Ahmed, D. Ventola, C. Daniel, Technical and economic analysis of solvent-based lithium-ion electrode drying with water and NMP, Drying Technology 36 (2018) 234–244. https://doi.org/10.1080/07373937.2017.1319855.
[32] S. Lee, E.-Y. Kim, H. Lee, E.-S. Oh, Effects of polymeric binders on electrochemical performances of spinel lithium manganese oxide cathodes in lithium ion batteries, Journal of Power Sources 269 (2014) 418–423. https://doi.org/10.1016/j.jpowsour.2014.06.167.
[33] P.P. Prosini, M. Carewska, C. Cento, A. Masci, Poly vinyl acetate used as a binder for the fabrication of a LiFePO4-based composite cathode for lithium-ion batteries, Electrochimica Acta 150 (2014) 129–135. https://doi.org/10.1016/j.electacta.2014.10.123.
[34] K. Soeda, M. Yamagata, M. Ishikawa, Alginic Acid as a New Aqueous Slurry-Based Binder for Cathode Materials of LIB, ECS Trans. 64 (2015) 13. https://doi.org/10.1149/06418.0013ecst.
[35] H. Isozumi, T. Horiba, K. Kubota, K. Hida, T. Matsuyama, S. Yasuno, S. Komaba, Application of modified styrene-butadiene-rubber-based latex binder to high-voltage operating LiCoO2 composite electrodes for lithium-ion batteries, Journal of Power Sources 468 (2020) 228332. https://doi.org/10.1016/j.jpowsour.2020.228332.
[36] L. Qiu, Z. Shao, D. Wang, W. Wang, F. Wang, J. Wang, Enhanced electrochemical properties of LiFePO4 (LFP) cathode using the carboxymethyl cellulose lithium (CMC-Li) as novel binder in lithium-ion battery, Carbohydrate Polymers 111 (2014) 588–591. https://doi.org/10.1016/j.carbpol.2014.05.027.
[37] F. Bigoni, F. De Giorgio, F. Soavi, C. Arbizzani, Sodium Alginate: A Water-Processable Binder in High-Voltage Cathode Formulations, Journal of The Electrochemical Society 164 (2017) A6171–A6177. https://doi.org/10.1149/2.0281701jes.
[38] J. Chong, S. Xun, H. Zheng, X. Song, G. Liu, P. Ridgway, J.Q. Wang, V.S. Battaglia, A comparative study of polyacrylic acid and poly(vinylidene difluoride) binders for spherical natural graphite/LiFePO4 electrodes and cells, Journal of Power Sources 196 (2011) 7707–7714. https://doi.org/10.1016/j.jpowsour.2011.04.043.
[39] M. Aslan, D. Weingarth, N. Jäckel, J.S. Atchison, I. Grobelsek, V. Presser, Polyvinylpyrrolidone as binder for castable supercapacitor electrodes with high electrochemical performance in organic electrolytes, Journal of Power Sources 266 (2014) 374–383. https://doi.org/10.1016/j.jpowsour.2014.05.031.
[40] H. Buqa, M. Holzapfel, F. Krumeich, C. Veit, P. Novák, Study of styrene butadiene rubber and sodium methyl cellulose as binder for negative

electrodes in lithium-ion batteries, Journal of Power Sources 161 (2006) 617–622. https://doi.org/10.1016/j.jpowsour.2006.03.073.
[41] R. Zhang, X. Yang, D. Zhang, H. Qiu, Q. Fu, H. Na, Z. Guo, F. Du, G. Chen, Y. Wei, Water soluble styrene butadiene rubber and sodium carboxyl methyl cellulose binder for ZnFe2O4 anode electrodes in lithium ion batteries, Journal of Power Sources 285 (2015) 227–234. https://doi.org/10.1016/j.jpowsour.2015.03.100.
[42] R. Gordon, R. Orias, N. Willenbacher, Effect of carboxymethyl cellulose on the flow behavior of lithium-ion battery anode slurries and the electrical as well as mechanical properties of corresponding dry layers, J Mater Sci 55 (2020) 15867–15881. https://doi.org/10.1007/s10853-020-05122-3.
[43] D. Versaci, R. Nasi, U. Zubair, J. Amici, M. Sgroi, M.A. Dumitrescu, C. Francia, S. Bodoardo, N. Penazzi, New eco-friendly low-cost binders for Li-ion anodes, J Solid State Electrochem 21 (2017) 3429–3435. https://doi.org/10.1007/s10008-017-3665-5.
[44] N. Yabuuchi, Y. Kinoshita, K. Misaki, T. Matsuyama, S. Komaba, Electrochemical Properties of LiCoO 2 Electrodes with Latex Binders on High-Voltage Exposure, J. Electrochem. Soc. 162 (2015) A538–A544. https://doi.org/10.1149/2.0151504jes.
[45] N. Yabuuchi, Y. Kinoshita, K. Misaki, T. Matsuyama, S. Komaba, Electrochemical Properties of LiCoO2 Electrodes with Latex Binders on High-Voltage Exposure, J. Electrochem. Soc. 162 (2015) A538–A544. https://doi.org/10.1149/2.0151504jes.
[46] Y. Qi, M.H.T. Nguyen, E.-S. Oh, Effect of conductive polypyrrole in poly(acrylonitrile-co-butyl acrylate) water–based binder on the performance of electrochemical double-layer capacitors, J Solid State Electrochem (2020). https://doi.org/10.1007/s10008-020-04864-z.
[47] M.H.T. Nguyen, E.-S. Oh, Application of a new acrylonitrile/butylacrylate water-based binder for negative electrodes of lithium-ion batteries, Electrochem Commun 35 (2013) 45–48. https://doi.org/10.1016/j.elecom.2013.07.042.
[48] S.S. Zhang, K. Xu, T.R. Jow, Electrochemical impedance study on the low temperature of Li-ion batteries, Electrochimica Acta 49 (2004) 1057–1061. https://doi.org/10.1016/j.electacta.2003.10.016.
[49] I.H. Son, J. Hwan Park, S. Kwon, S. Park, M.H. Rümmeli, A. Bachmatiuk, H.J. Song, J. Ku, J.W. Choi, J. Choi, S.-G. Doo, H. Chang, Silicon carbide-free graphene growth on silicon for lithium-ion battery with high volumetric energy density, Nature Communications 6 (2015) 1–8. https://doi.org/10.1038/ncomms8393.

[50] H. Wu, Y. Cui, Designing nanostructured Si anodes for high energy lithium ion batteries, Nano Today 7 (2012) 414–429. https://doi.org/10.1016/j.nantod.2012.08.004.
[51] X. Li, M. Gu, S. Hu, R. Kennard, P. Yan, X. Chen, C. Wang, M.J. Sailor, J.-G. Zhang, J. Liu, Mesoporous silicon sponge as an anti-pulverization structure for high-performance lithium-ion battery anodes, Nature Communications 5 (2014) 1–7. https://doi.org/10.1038/ncomms5105.
[52] Z. Yu, N. Wang, S. Fang, X. Qi, Z. Gao, J. Yang, S. Lu, Pilot-Plant Production of High-Performance Silicon Nanowires by Molten Salt Electrolysis of Silica, Industrial & Engineering Chemistry Research (2019). https://doi.org/10.1021/acs.iecr.9b04430.
[53] H. Wang, J. Fu, C. Wang, J. Wang, A. Yang, C. Li, Q. Sun, Y. Cui, H. Li, A binder-free high silicon content flexible anode for Li-ion batteries, Energy & Environmental Science 13 (2020) 848–858. https://doi.org/10.1039/C9EE02615K.
[54] C. Qi, S. Li, Z. Yang, Z. Xiao, L. Zhao, F. Yang, G. Ning, X. Ma, C. Wang, J. Xu, J. Gao, Suitable thickness of carbon coating layers for silicon anode, Carbon 186 (2022) 530–538. https://doi.org/10.1016/j.carbon.2021.10.062.
[55] Q. Huang, J. Song, Y. Gao, D. Wang, S. Liu, S. Peng, C. Usher, A. Goliaszewski, D. Wang, Supremely elastic gel polymer electrolyte enables a reliable electrode structure for silicon-based anodes, Nature Communications 10 (2019) 1–7. https://doi.org/10.1038/s41467-019-13434-5.
[56] J. Chen, A. Naveed, Y. NuLi, J. Yang, J. Wang, Designing an intrinsically safe organic electrolyte for rechargeable batteries, Energy Storage Materials 31 (2020) 382–400. https://doi.org/10.1016/j.ensm.2020.06.027.
[57] J. Chen, X. Fan, Q. Li, H. Yang, M.R. Khoshi, Y. Xu, S. Hwang, L. Chen, X. Ji, C. Yang, H. He, C. Wang, E. Garfunkel, D. Su, O. Borodin, C. Wang, Electrolyte design for LiF-rich solid–electrolyte interfaces to enable high-performance microsized alloy anodes for batteries, Nature Energy 5 (2020) 386–397. https://doi.org/10.1038/s41560-020-0601-1.
[58] Z. Shi, Q. Liu, Z. Yang, L.A. Robertson, S.R. Bheemireddy, Y. Zhao, Z. Zhang, L. Zhang, A chemical switch enabled autonomous two-stage crosslinking polymeric binder for high performance silicon anodes, Journal of Materials Chemistry A 10 (2022) 1380–1389. https://doi.org/10.1039/D1TA07112B.
[59] S. Niu, M. Zhao, L. Ma, F. Zhao, Y. Zhang, G. Tang, Y. Wang, A. Pang, W. Li, L. Wei, High performance polyurethane–polyacrylic acid polymer binders for silicon microparticle anodes in lithium-ion batteries, Sustainable Energy & Fuels (2022). https://doi.org/10.1039/D1SE01820E.

[60] Y. Wang, H. Xu, X. Chen, Novel constructive self-healing binder for silicon anodes with high mass loading in lithium-ion batteries, Energy Storage Materials 38 (2021) 121–129. https://doi.org/10.1016/j.ensm.2021.03.003.
[61] T. Kwon, J.W. Choi, A. Coskun, The emerging era of supramolecular polymeric binders in silicon anodes, Chemical Society Reviews 47 (2018) 2145–2164. https://doi.org/10.1039/C7CS00858A.
[62] J. Nam, E. Kim, R. K. K., Y. Kim, T.-H. Kim, A conductive self healing polymeric binder using hydrogen bonding for Si anodes in lithium ion batteries, Scientific Reports 10 (2020) 1–12. https://doi.org/10.1038/s41598-020-71625-3.
[63] Y.-M. Zhao, F.-S. Yue, S.-C. Li, Y. Zhang, Z.-R. Tian, Q. Xu, S. Xin, Y.-G. Guo, Advances of polymer binders for silicon-based anodes in high energy density lithium-ion batteries, InfoMat 3 (2021) 460–501. https://doi.org/10.1002/inf2.12185.
[64] Y. Yu, J. Zhu, K. Zeng, M. Jiang, Mechanically robust and superior conductive n-type polymer binders for high-performance micro-silicon anodes in lithium-ion batteries, Journal of Materials Chemistry A 9 (2021) 3472–3481. https://doi.org/10.1039/D0TA10525B.
[65] S. Cao, B. Shen, T. Tong, J. Fu, J. Yu, 2D/2D Heterojunction of Ultrathin MXene/Bi2WO6 Nanosheets for Improved Photocatalytic CO2 Reduction, Advanced Functional Materials 28 (2018) 1800136. https://doi.org/10.1002/adfm.201800136.
[66] J. Zhang, Y. Zhao, X. Guo, C. Chen, C.-L. Dong, R.-S. Liu, C.-P. Han, Y. Li, Y. Gogotsi, G. Wang, Single platinum atoms immobilized on an MXene as an efficient catalyst for the hydrogen evolution reaction, Nature Catalysis 1 (2018) 985–992. https://doi.org/10.1038/s41929-018-0195-1.
[67] S. Song, C. Zhang, W. Li, J. Wang, P. Rao, J. Wang, T. Li, Y. Zhang, Bioinspired engineering of gradient and hierarchical architecture into pressure sensors toward high sensitivity within ultra-broad working range, Nano Energy 100 (2022) 107513. https://doi.org/10.1016/j.nanoen.2022.107513.
[68] X. Wu, H. Liao, D. Ma, M. Chao, Y. Wang, X. Jia, P. Wan, L. Zhang, A wearable, self-adhesive, long-lastingly moist and healable epidermal sensor assembled from conductive MXene nanocomposites, Journal of Materials Chemistry C 8 (2020) 1788–1795. https://doi.org/10.1039/C9TC05575D.
[69] J. Pang, R.G. Mendes, A. Bachmatiuk, L. Zhao, H.Q. Ta, T. Gemming, H. Liu, Z. Liu, M.H. Rummeli, Applications of 2D MXenes in energy conversion and storage systems, Chemical Society Reviews 48 (2019) 72–133. https://doi.org/10.1039/C8CS00324F.
[70] Q. Yang, Y. Wang, X. Li, H. Li, Z. Wang, Z. Tang, L. Ma, F. Mo, C. Zhi, Recent Progress of MXene-Based Nanomaterials in Flexible Energy Storage

and Electronic Devices, Energy & Environmental Materials 1 (2018) 183–195. https://doi.org/10.1002/eem2.12023.
[71] M. Naguib, M. Kurtoglu, V. Presser, J. Lu, J. Niu, M. Heon, L. Hultman, Y. Gogotsi, M.W. Barsoum, Two-Dimensional Nanocrystals Produced by Exfoliation of Ti3AlC2, Advanced Materials 23 (2011) 4248–4253. https://doi.org/10.1002/adma.201102306.
[72] M. Naguib, O. Mashtalir, J. Carle, V. Presser, J. Lu, L. Hultman, Y. Gogotsi, M.W. Barsoum, Two-Dimensional Transition Metal Carbides, ACS Nano (2012). https://doi.org/10.1021/nn204153h.
[73] R.M. Ronchi, J.T. Arantes, S.F. Santos, Synthesis, structure, properties and applications of MXenes: Current status and perspectives, Ceramics International 45 (2019) 18167–18188. https://doi.org/10.1016/j.ceramint.2019.06.114.
[74] Q. Pan, Y. Zheng, S. Kota, W. Huang, S. Wang, H. Qi, S. Kim, Y. Tu, M.W. Barsoum, C.Y. Li, 2D MXene-containing polymer electrolytes for all-solid-state lithium metal batteries, Nanoscale Advances 1 (2019) 395–402. https://doi.org/10.1039/C8NA00206A.
[75] H. Xu, X. Yin, X. Li, M. Li, S. Liang, L. Zhang, L. Cheng, Lightweight Ti2CTx MXene/Poly(vinyl alcohol) Composite Foams for Electromagnetic Wave Shielding with Absorption-Dominated Feature, ACS Applied Materials & Interfaces (2019). https://doi.org/10.1021/acsami.8b21671.
[76] X. Huang, R. Wang, T. Jiao, G. Zou, F. Zhan, J. Yin, L. Zhang, J. Zhou, Q. Peng, Facile Preparation of Hierarchical AgNP-Loaded MXene/Fe3O4/Polymer Nanocomposites by Electrospinning with Enhanced Catalytic Performance for Wastewater Treatment, ACS Omega (2019). https://doi.org/10.1021/acsomega.8b03615.
[77] S. Tu, Q. Jiang, X. Zhang, H.N. Alshareef, Large Dielectric Constant Enhancement in MXene Percolative Polymer Composites, ACS Nano (2018). https://doi.org/10.1021/acsnano.7b08895.
[78] Z. Ling, C.E. Ren, M.-Q. Zhao, J. Yang, J.M. Giammarco, J. Qiu, M.W. Barsoum, Y. Gogotsi, Flexible and conductive MXene films and nanocomposites with high capacitance, Proceedings of the National Academy of Sciences 111 (2014) 16676–16681. https://doi.org/10.1073/pnas.1414215111.
[79] R. Sun, H.-B. Zhang, J. Liu, X. Xie, R. Yang, Y. Li, S. Hong, Z.-Z. Yu, Highly Conductive Transition Metal Carbide/Carbonitride(MXene)@polystyrene Nanocomposites Fabricated by Electrostatic Assembly for Highly Efficient Electromagnetic Interference Shielding, Advanced Functional Materials 27 (2017) 1702807. https://doi.org/10.1002/adfm.201702807.

[80] J. Yang, W. Bao, P. Jaumaux, S. Zhang, C. Wang, G. Wang, MXene-Based Composites: Synthesis and Applications in Rechargeable Batteries and Supercapacitors, Advanced Materials Interfaces 6 (2019) 1802004. https://doi.org/10.1002/admi.201802004.
[81] Y. Liao, W. Li, M.M. Rao, Fumed silica-doped poly(butyl methacrylate-styrene)-based gel polymer electrolyte for lithium ion battery, Journal of Membrane Science 352 (2010) 95–99. https://doi.org/10.1016/j.memsci.2010.01.064.
[82] J.T. Lee, Y. Chu, X. Peng, C. Li, A novel and efficient water-based composite binder for LiCoO2 cathodes in lithium-ion batteries, Journal of Power Sources 173 (2007) 985–989. https://doi.org/10.1016/j.jpowsour.2007.07.073.
[83] C.-D. Yuan, A.-H. Miao, J.-W. Cao, Y.-S. Xu, T.-Y. Cao, Preparation of monodispersed hollow polymer particles by seeded emulsion polymerization under low emulsifier conditions, Journal of Applied Polymer Science 98 (2005) 1505–1510. https://doi.org/10.1002/app.21971.
[84] Y. Huang, Y. Huang, B. Liu, H. Cao, L. Zhao, Gel polymer electrolyte based on p(acrylonitrile-maleic anhydride) for lithium ion battery, Electrochimica Acta 286 (2018) 242–251. https://doi.org/10.1016/j.electacta.2018.08.024.
[85] Y. Liao, D. Zhou, M.M. Rao, W. Li, Z. Cai, Self-supported poly(methyl methacrylate–acrylonitrile–vinyl acetate)-based gel electrolyte for lithium ion battery, Journal of Power Sources 189 (2009) 139–144. https://doi.org/10.1016/j.jpowsour.2008.10.027.
[86] Y. Gao, X. Qiu, X. Wang, A. Gu, L. Zhang, X. Chen, J. Li, Z. Yu, Chitosan-g-Poly(acrylic acid) Copolymer and Its Sodium Salt as Stabilized Aqueous Binders for Silicon Anodes in Lithium-Ion Batteries, ACS Sustainable Chemistry & Engineering (2019). https://doi.org/10.1021/acssuschemeng.9b03307.
[87] S.-Y. Jang, S.-H. Han, Fabrication of Si negative electrodes for Li-ion batteries (LIBs) using cross-linked polymer binders, Scientific Reports 6 (2016) 1–9. https://doi.org/10.1038/srep38050.
[88] L. Zhao, Z. Sun, H. Zhang, Y. Li, Y. Mo, F. Yu, Y. Chen, An environment-friendly crosslinked binder endowing LiFePO 4 electrode with structural integrity and long cycle life performance, RSC Advances 10 (2020) 29362–29372. https://doi.org/10.1039/D0RA05095D.
[89] S. Lee, Y.C. Choi, S.-H. Kwon, J.-S. Bae, E.D. Jeong, Cracking resistance and electrochemical performance of silicon anode on binders with different mechanical characteristics, Journal of Industrial and Engineering Chemistry 74 (2019) 216–222. https://doi.org/10.1016/j.jiec.2019.03.009.
[90] S. Komaba, K. Shimomura, N. Yabuuchi, T. Ozeki, H. Yui, K. Konno, Study on Polymer Binders for High-Capacity SiO Negative Electrode of Li-Ion

Batteries, The Journal of Physical Chemistry C (2011). https://doi.org/10.1021/jp201691g.
[91] J. Zhang, B. Sun, X. Huang, S. Chen, G. Wang, Honeycomb-like porous gel polymer electrolyte membrane for lithium ion batteries with enhanced safety, Scientific Reports 4 (2014) 1–7. https://doi.org/10.1038/srep06007.
[92] B. M, A. Sb, R.S. S, H. Mh, M. Sr, A. Rt, K. Mfz, A. Rm, Energy Storage Behavior of Lithium-Ion Conducting poly(vinyl alcohol) (PVA): Chitosan(CS)-Based Polymer Blend Electrolyte Membranes: Preparation, Equivalent Circuit Modeling, Ion Transport Parameters, and Dielectric Properties, Membranes 10 (2020). https://doi.org/10.3390/membranes10120381.
[93] D. Bérardan, S. Franger, A. K. Meena, N. Dragoe, Room temperature lithium superionic conductivity in high entropy oxides, Journal of Materials Chemistry A 4 (2016) 9536–9541. https://doi.org/10.1039/C6TA03249D.
[94] N. Kamaya, K. Homma, Y. Yamakawa, M. Hirayama, R. Kanno, M. Yonemura, T. Kamiyama, Y. Kato, S. Hama, K. Kawamoto, A. Mitsui, A lithium superionic conductor, Nature Materials 10 (2011) 682–686. https://doi.org/10.1038/nmat3066.
[95] C. Luo, L. Du, W. Wu, H. Xu, G. Zhang, S. Li, C. Wang, Z. Lu, Y. Deng, Novel Lignin-Derived Water-Soluble Binder for Micro Silicon Anode in Lithium-Ion Batteries, ACS Sustainable Chemistry & Engineering (2018). https://doi.org/10.1021/acssuschemeng.8b01161.
[96] Z.H. Xie, M.Z. Rong, M.Q. Zhang, Dynamically Cross-Linked Polymeric Binder-Made Durable Silicon Anode of a Wide Operating Temperature Li-Ion Battery, ACS Applied Materials & Interfaces 13 (2021) 28737–28748. https://doi.org/10.1021/acsami.1c01472.
[97] Z. Wang, T. Huang, A. Yu, A carboxymethyl vegetable gum as a robust water soluble binder for silicon anodes in lithium-ion batteries, Journal of Power Sources 489 (2021) 229530. https://doi.org/10.1016/j.jpowsour.2021.229530.
[98] G.S. Gund, J. Park, H. Park, Y. Gogotsi, MXene/Polymer Hybrid Materials for Flexible AC-Filtering Electrochemical Capacitors, Joule 3 (2019) 164–176. https://doi.org/10.1016/j.joule.2018.10.017.
[99] L. Han, T. Liu, O. Sheng, Y. Liu, Y. Wang, J. Nai, L. Zhang, X. Tao, Undervalued Roles of Binder in Modulating Solid Electrolyte Interphase Formation of Silicon-Based Anode Materials, ACS Applied Materials & Interfaces (2021). https://doi.org/10.1021/acsami.1c13971.
[100] T. Munaoka, X. Yan, J. Lopez, J.W.F. To, J. Park, J.B.-H. Tok, Y. Cui, Z. Bao, Ionically Conductive Self-Healing Binder for Low Cost Si Microparticles Anodes in Li-Ion Batteries, Advanced Energy Materials 8 (2018) 1703138. https://doi.org/10.1002/aenm.201703138.

[101] S. Hu, L. Wang, T. Huang, A. Yu, A conductive self-healing hydrogel binder for high-performance silicon anodes in lithium-ion batteries, Journal of Power Sources 449 (2020) 227472. https://doi.org/10.1016/j.jpowsour.2019.227472.
[102] M. Zheng, C. Wang, Y. Xu, K. Li, D. Liu, A water-soluble binary conductive binder for Si anode lithium ion battery, Electrochimica Acta 305 (2019) 555–562. https://doi.org/10.1016/j.electacta.2019.02.080.
[103] Y. Zhao, L. Yang, Y. Zuo, Z. Song, F. Liu, K. Li, F. Pan, Conductive Binder for Si Anode with Boosted Charge Transfer Capability via n-Type Doping, ACS Applied Materials & Interfaces (2018). https://doi.org/10.1021/acsami.8b08843.
[104] Y. Xie, M. Naguib, V.N. Mochalin, M.W. Barsoum, Y. Gogotsi, X. Yu, K.-W. Nam, X.-Q. Yang, A.I. Kolesnikov, P.R.C. Kent, Role of Surface Structure on Li-Ion Energy Storage Capacity of Two-Dimensional Transition-Metal Carbides, Journal of the American Chemical Society 136 (2014) 6385–6394. https://doi.org/10.1021/ja501520b.
[105] J. Song, M. Zhou, R. Yi, T. Xu, M.L. Gordin, D. Tang, Z. Yu, M. Regula, D. Wang, Interpenetrated Gel Polymer Binder for High-Performance Silicon Anodes in Lithium-ion Batteries, Advanced Functional Materials 24 (2014) 5904–5910. https://doi.org/10.1002/adfm.201401269.
[106] X. Li, M. Zhang, S. Yuan, C. Lu, Research Progress of Silicon/Carbon Anode Materials for Lithium-Ion Batteries: Structure Design and Synthesis Method, ChemElectroChem 7 (2020) 4289–4302. https://doi.org/10.1002/celc.202001060.
[107] Y. Qi, G. Wang, S. Li, T. Liu, J. Qiu, H. Li, Recent progress of structural designs of silicon for performance-enhanced lithium-ion batteries, Chemical Engineering Journal 397 (2020) 125380. https://doi.org/10.1016/j.cej.2020.125380.
[108] M.-H. Park, M.G. Kim, J. Joo, K. Kim, J. Kim, S. Ahn, Y. Cui, J. Cho, Silicon Nanotube Battery Anodes, Nano Lett. 9 (2009) 3844–3847. https://doi.org/10.1021/nl902058c.
[109] M. Ling, Y. Xu, H. Zhao, X. Gu, J. Qiu, S. Li, M. Wu, X. Song, C. Yan, G. Liu, S. Zhang, Dual-functional gum arabic binder for silicon anodes in lithium ion batteries, Nano Energy 12 (2015) 178–185. https://doi.org/10.1016/j.nanoen.2014.12.011.
[110] S. Chae, S.-H. Choi, N. Kim, J. Sung, J. Cho, Integration of Graphite and Silicon Anodes for the Commercialization of High-Energy Lithium-Ion Batteries, Angewandte Chemie International Edition 59 (2020) 110–135. https://doi.org/10.1002/anie.201902085.

[111] J.-Y. Li, Q. Xu, G. Li, Y.-X. Yin, L.-J. Wan, Y.-G. Guo, Research progress regarding Si-based anode materials towards practical application in high energy density Li-ion batteries, Mater. Chem. Front. 1 (2017) 1691–1708. https://doi.org/10.1039/C6QM00302H.
[112] Y. Jin, S. Li, A. Kushima, X. Zheng, Y. Sun, J. Xie, J. Sun, W. Xue, G. Zhou, J. Wu, F. Shi, R. Zhang, Z. Zhu, K. So, Y. Cui, J. Li, Self-healing SEI enables full-cell cycling of a silicon-majority anode with a coulombic efficiency exceeding 99.9%, Energy Environ. Sci. 10 (2017) 580–592. https://doi.org/10.1039/C6EE02685K.
[113] C.K. Chan, H. Peng, G. Liu, K. McIlwrath, X.F. Zhang, R.A. Huggins, Y. Cui, High-performance lithium battery anodes using silicon nanowires, Nature Nanotech 3 (2008) 31–35. https://doi.org/10.1038/nnano.2007.411.
[114] H.S. Choi, J.G. Lee, H.Y. Lee, S.W. Kim, C.R. Park, Effects of surrounding confinements of Si nanoparticles on Si-based anode performance for lithium ion batteries, Electrochimica Acta 56 (2010) 790–796. https://doi.org/10.1016/j.electacta.2010.09.101.
[115] M. Su, Z. Wang, H. Guo, X. Li, S. Huang, W. Xiao, L. Gan, Enhancement of the Cyclability of a Si/Graphite@Graphene composite as anode for Lithium-ion batteries, Electrochimica Acta 116 (2014) 230–236. https://doi.org/10.1016/j.electacta.2013.10.195.
[116] P. Li, H. Kim, S.-T. Myung, Y.-K. Sun, Diverting Exploration of Silicon Anode into Practical Way: A Review Focused on Silicon-Graphite Composite for Lithium Ion Batteries, Energy Storage Materials 35 (2021) 550–576. https://doi.org/10.1016/j.ensm.2020.11.028.
[117] M. Tian, Y. Qi, E.-S. Oh, Application of a Polyacrylate Latex to a Lithium Iron Phosphate Cathode as a Binder Material, Energies 14 (2021) 1902. https://doi.org/10.3390/en14071902.
[118] Z. Shi, S. Jiang, L.A. Robertson, Y. Zhao, E. Sarnello, T. Li, W. Chen, Z. Zhang, L. Zhang, Restorable Neutralization of Poly(acrylic acid) Binders toward Balanced Processing Properties and Cycling Performance for Silicon Anodes in Lithium-Ion Batteries, ACS Appl. Mater. Interfaces 12 (2020) 57932–57940. https://doi.org/10.1021/acsami.0c18559.
[119] D.-E. Yoon, C. Hwang, N.-R. Kang, U. Lee, D. Ahn, J.-Y. Kim, H.-K. Song, Dependency of Electrochemical Performances of Silicon Lithium-Ion Batteries on Glycosidic Linkages of Polysaccharide Binders, ACS Appl. Mater. Interfaces 8 (2016) 4042–4047. https://doi.org/10.1021/acsami.5b11408.
[120] L. Qiu, Z. Shao, D. Wang, F. Wang, W. Wang, J. Wang, Carboxymethyl cellulose lithium (CMC-Li) as a novel binder and its electrochemical

performance in lithium-ion batteries, Cellulose 21 (2014) 2789–2796. https://doi.org/10.1007/s10570-014-0274-7.
[121] S. Choi, T. Kwon, A. Coskun, J.W. Choi, Highly elastic binders integrating polyrotaxanes for silicon microparticle anodes in lithium ion batteries, Science 357 (2017) 279–283. https://doi.org/10.1126/science.aal4373.
[122] S. Jiang, B. Hu, Z. Shi, W. Chen, Z. Zhang, L. Zhang, Re-Engineering Poly(Acrylic Acid) Binder toward Optimized Electrochemical Performance for Silicon Lithium-Ion Batteries: Branching Architecture Leads to Balanced Properties of Polymeric Binders, Advanced Functional Materials 30 (2020) 1908558. https://doi.org/10.1002/adfm.201908558.
[123] Z. Cai, S. Hu, Y. Wei, T. Huang, A. Yu, H. Zhang, In Situ Room-Temperature Cross-Linked Highly Branched Biopolymeric Binder Based on the Diels–Alder Reaction for High-Performance Silicon Anodes in Lithium-Ion Batteries, ACS Appl. Mater. Interfaces 13 (2021) 56095–56108. https://doi.org/10.1021/acsami.1c16196.
[124] Y. Ma, K. Chen, J. Ma, G. Xu, S. Dong, B. Chen, J. Li, Z. Chen, X. Zhou, G. Cui, A biomass based free radical scavenger binder endowing a compatible cathode interface for 5 V lithium-ion batteries, Energy & Environmental Science 12 (2019) 273–280. https://doi.org/10.1039/C8EE02555J.
[125] Y. Ohkatsu, T. Matsuura, M. Yamato, A phenolic antioxidant trapping both alkyl and peroxy radicals, Polymer Degradation and Stability 81 (2003) 151–156. https://doi.org/10.1016/S0141-3910(03)00084-3.